A THESIS

FOR THE DEGREE OF DOCTOR OF PHILOSOPHY

Liver-on-Chip Development for Pathophysiological Emulation and Drug Toxicity Testing

GRADUATE SCHOOL

JEJU NATIOANL UNIVERSITY

DEPARTMENT OF MECHATRONICS ENGINEERING

Hafiz Muhammad Umer Farooqi

February 2022

Liver-on-Chip Development for Pathophysiological Emulation and Drug Toxicity Testing

Hafiz Muhammad Umer Farooqi
(Supervised by Professor Dr. Kyung Hyun Choi)

A thesis submitted in partial fulfillment of the requirements for the degree of
Doctor of Philosophy
February 2022
This thesis has been examined and approved.

Jong Hwan Lim
Thesis Committee Chair, **Prof. Jong Hwan Lim,**
Mechatronics Engineering Department

Thesis Committee Vice-Chair, **Prof. Chul Ung Kang,**
Mechatronics Engineering Department

Thesis Committee Member, **Prof. Sun Ryung Lee,**
Biology Department

Thesis Committee Member, **Prof. Sang Ho Lee,**
Pharmacy Department

Thesis Director, **Prof. Kyung Hyun Choi,**
Mechatronics Engineering Department

DEPARTMENT OF MECHATRONICS ENGINEERING
GRADUATE SCHOOL
JEJU NATIONAL UNIVERSITY

Preamble

This thesis is submitted for the degree of Doctor of Engineering in the Department of Mechatronics Engineering, Jeju National University, South Korea. No content or segment of this thesis has been submitted for any degree at any other institution or university. This thesis work is original according to the best of the author's knowledge unless reference is taken from the published work. This thesis has been published or submitted in different international journal articles written originally by the author. A list of related published in different international journal articles, written by the author. A list of related publications is given below:

1. Farooqi, H.M.U.; Khalid, M.A.U.; Kim, H.H.; Lee, S.R.; Choi, K.H. "Real-time physiological sensor-based liver-on-chip device for monitoring drug toxicity". **Journal of Micromechanics and Microengineering**, 30, 115013
2. Farooqi, H.M.U.; Kang, B.; Khalid, M.A.U.; Salih, A.R.C.; Hyun, K.; S.H.; Huh, D.; Choi, K.H. Real-time monitoring of liver fibrosis through embedded sensors in a microphysiological system. **Nano Convergence**, 2021,8,3.

Dedication

Dedicated to my beloved wife, Fatima, and adorable sons, Dawood & Yousuf, who sacrificed and suffered a lot during the journey of my doctoral studies, my loving parents without whom this journey would not have been possible, And to my spiritual mentors Hazrat Umer-e-Farooq (RA), Data Ganj Baksh (RA), Hazrat Naqashband Bahauddin Bokhari (RA), Hazrat Shaikh Ahmad Sarhindi (RA), Pir Mehar Ali Shah (RA), Hafiz Abdul Kareem Naqshbandi (RA), Baba Ji Qasim Moharwi (RA) and Hazrat Saeed Ahmad Mojaddadi (RA)!

Acknowledgments

Starting with my gratitude to Allah Almighty worthy of all praises, for the one, he is the only true God, and Prophet Muhammad (PBUH) is the last Prophet of Allah. If not for their continuous help, grace, and support, I would never have been where I am today. They have been showing the righteous path in the toughest of times and situations. May their blessings be always shown on my family and me. I pray to Allah to always be merciful and guide me in the quest for scientific advancements and contribute to the betterment of humanity.

Secondly, I would like to thank my parents, siblings (Tuba, Ali, Awais, Umer, Ahmad, Habib), wife, and beloved sons, without whom this journey would have been impossible. They have always believed in me, encouraged me, and supported me through tough times. I remember the hard times that my family had gone through. Still, my parents always stood their ground to support me financially and emotionally throughout my studies, and this achievement is an ultimate result of their contributions and effort. Finally, I would express my gratitude to my fast friends Sohail Aslam Sheikh, Luqman Zafar, Kamran Aslam, Yasir Nasir, Asif Raza, Imran Khan, Yaseen Farooqi, Abuzar Farooqi, Abdullah Zaki, Muhammad Aslam, Waheed Rasheed, Hasanain Haider, for keeping in touch during this whole time.

I want to take this opportunity to thank my Ph.D. advisor, Prof. Kyung Hyun Choi, for his ultimate guidance and support throughout my degree program. He also played the role of a loving father and grandfather for my kids and me. He always kept me motivated and made me pass through the boundaries to expand my scientific & societal knowledge and perform best in academic research. Furthermore, I would like to thank all my teachers, especially Prof. Dong Guk Paeng, for their ever-lasting contributions to my achievements. I wish all of them excellent health and a happier life.

I am grateful to my seniors and brotherly figures for helping me out during my academic and research career, to name a few: Dr. Shahid Aziz, Dr. Nilesh Kumar Meghani, and Dr. Mohanraj Murugesan. I am also thankful to my colleague at Advanced Micro Mechatronics Lab, Dr. Muhsin Ali, Chethikkattuveli Salih Abdul Rahim, Kinam Hyun, all other lab members. A great thanks to my friends, including Imran Jamal, Muhammad Asif, Shinawar Ali Khan, Krishna Singh Bhandari, Jiyoun Kim, Minhu Han, Hyeong Geyon Kim, Karuppasamy Sivasubramanian Abisegapriyan, Choon Take Cho (Ge Hay), Mr. Lee and Waseem Raza.

In the end, I would like to thank the great nation and people of the Republic of Korea, their government, and Jeju-do's remarkable inhabitants for making my stay at Jeju Island comfortable, peaceful, and joyous. The years I spent here in Jeju-do will forever cherish in my memories. I want to revisit Korea and especially Jeju occasionally to live those good memories all over again.

Hafiz Muhammad Umer Farooqi

February 2022

Contents

List of Figures

List of Tables

Abstract

The liver is a vital organ and plays a crucial role in the homeostasis of the human body. Detoxification, metabolism, nutrient storage, hemopoiesis, and synthesis of essential biomolecules are its core functions. Hepatic enzymes are specialized in drug metabolism and biotransformation. In comparison, hepatocytes assimilate metabolites and produce several types of cytokines and proteins. Food, aging, environment, and lifestyle directly influence the liver's health. Cancer, viral infections, alcohol abuse, and metabolic syndromes are the leading causes of hepatic pathologies. Animals and cell culture models are employed to model and investigate hepatic anomalies and therapeutics. However, genetic variation, ethical issues, and higher costs are limiting animal testing in medicine. In comparison, cell culture models exhibit poor translation capacity due to a lack of peculiar in vivo hepatic microenvironment. Therefore, this research pivots the development of a microfluidic-based in vitro liver model to overcome the ethical and translational issues. In this thesis, the focus was given to creating a liver-on-chip for modeling liver diseases and testing various pharmaceutical substances. Human hepatocytes were used to develop a liver-on-chip model, and it was monitored with embedded sensors. As a result, hepatic fibrosis modeling and anticancer drug toxicity were successfully performed, and a novel method of fibrosis developmental study was introduced. In brief, liver-on-chip is a promising model that can aid and overcome the challenges faced by clinicians and researchers in reverse engineering, translation medicine, precision medicine, and drug discovery.

1. Objectives of Thesis

The primary object of this thesis was to develop a glass chip-based microfluidic liver-on-chip device and organ-on-chip platform for drug toxicity testing and disease modeling. Additionally, the development and the implementation of the non-invasive and chip embedded biosensors for real-time monitoring of organ-on-chip devices to surpass traditional expensive and laborious end point bioassays. Furthermore, to facilitate extracellular matrix application, cell staining, and cell seeding for organ-on-chip devices by developing a custom-made cell seeding kit. This study was also carried out to take advantage from 3D printing technology for organ-on -chip applications.

2. Introduction

2.1. Organ-on-Chip

The science of microfluidics accurately controls and manipulates fluids. The application of controlled microfluidics by applying microchannels is called lab-on-a-chip. Though the microchannels are tiny, they offer large surface area and mass transfer, aiding their applications in microfluidics for less reagent utility, controlled volumes, macromixing, shear stress, and physiochemical controls.[1] Microfluidics significantly increased the efficacy of sample preparation, chemical reaction kinetics, physical separation, biological detection, cell manipulation, and sensors. Organ-on-chip (OOC) is a subbranch of lab-on-a-chip, in which biological organs are grown at a microscale by keeping their physiological and histological phenotype. OOC is often termed as the reverse engineering or *in vitro* biomimicking of organs. OOC offers precise control on shear stress, a vital parameter for optimum cell differentiation, division, and propagation.[2] The micro scaling of animal organs is promising in studying drug-drug interactions, substance toxicity, organ-organ crosstalk, physiochemical or physio electrical stimulant response, and genetics.

The study of the pathophysiology of the human body is the fundamental pillar of drug development and medical innovations. The most applied methods used for this purpose are *in vivo* and *in vitro* models. Animals are widely used for drug testing and medical interventions, which is continuously raising ethical concerns.[3] Additionally, animal models lack human genotyping and cannot predict or translate the actual human response of the analyte. Furthermore, the biological process requires a complex interaction between organs, body fluids, proteins, and biological molecules, which vary from species to species.[4] Hence, the drug regulatory bodies are discouraging the use of animal models for biomedical research. In pharmaceutical research, hundreds and thousands of candidate

compounds need to be examined for efficacy, safety, and toxicity, which is practically and economically impossible with animal models. Hence, the *in vitro* models are applied for this purpose.[5] Researchers prefer traditional cell culture models due to their usability for high throughput testing capacity. Cell culture is the method of harvesting cells from living bodies and then their propagation and growth and is called two-dimensional (2D) cell cultures. Unfortunately, traditional cell cultures lack the peculiar *in vivo* microenvironment characterized by a complex lattice of extracellular matrix (ECM) and specific shear stress induced by biological fluids.[6]

Hence, traditional cell cultures often require the translation of biological experiments with animal models to validate the experiments. At the same time, animal testing is prone to misleading information regarding drug toxicity and efficacy due to the species differences and lack of genetic similarity to humans. Moreover, animal models also come with ethical issues and high costs.[7] The inadequate information of the drug interaction with biological systems at preclinical drug testing leads to the failure of candidate drugs at the clinical stage and the loss of precious human lives.[8] OOC has rolled out these limitations of the traditional *in vivo* and *in vitro* models by offering humanized organ models. OOCs are customizable, micro-controlled, compact, physiologically more relevant than other traditional in vitro models, and offer the integration of several gadgets for mechanical and electrical stimulation.[9] Additionally, OOC technology offers multi-organ study of biological phenomena by connecting the various organs through microfluidic connections and microchannels. So far, lung, gut, brain, tooth, tongue, kidney, heart, skin, spleen, lymph node, eye, hair, cochlea, ovary, testis, breast, bone, and several other organs have been successfully translated and reverse-engineered using the OOC technology. Some

human-on-chip models are also introduced for studying pharmacokinetics (pk) and pharmacodynamics (pd) of drugs through connecting various organ chips or by growing several organs on a single microfluidic chip.[10] Thus, OOC is now considered the future substitute for animal testing for drug testing, personalized medicine, reverse engineering, and disease modeling.

Table 2-1. Shear stress values of various human organs

Sr No.	**Tissue**	**Cell Name**	**Shear Stress dyn cm^{-2}**	**References**
1	Liver	Hepatocytes (Human Embryonic Stem Cells)	0.1-0.05	[11]
		Hepatocytes	< 2	[12]
2	Kidney	Human Proximal Tubular Cells	0.2	[13]
		Glomerular Epithelial Cells	0.7-1.2	[14]
3	Lung	Alveolar Epithelial Cells	8-15	[15]
		A549 Cell Line	4-20	[16]
4	Uterus	HeLa Cell Line	25	[12]
5	Breast	MCF-7 Cell Line	1.4-16	[12]
6	Brain	Human Neural Stem Cells	0.0005	[12]
		HumanSY5Y Cells	0.001- 4	[12]
7	Muscle	C2C12 Myoblasts	0.05-0.7	[12]
8	Bone	MC3T3-EI Osteoblasts	0.001-4	[12]
9	Gut	Caco-2	0.025	[17]
10	Adipose Tissue	3T3-L1 Adipocyte	0.001-4	[12]

2.2. Liver-on-Chip

The liver is one of the vital organs of the human body and plays an indispensable role in multiple allied functions for physiological homeostasis, such as lipid and carbohydrate metabolism, protein synthesis, and detoxification of compounds. Physiologically, the liver has the potential to regenerate after encountering physiochemical injury and excision.[18] However, the pathology induced by severe stresses such as drugs (e.g., non-steroidal anti-inflammatory drugs, acetaminophen) and chronic diseases (e.g., fibrosis, hepatitis) limits its capability to carry out physiochemical tasks.

Currently, mammalian *in vivo* models are rampant to investigate the liver pathophysiology in pharmaceutics and disease modeling.[19] However, the translational capacity of *in vivo* models is poor and often fails the candidate drugs at the clinical stages of drug development. Nearly half of the candidate drug compounds were behind the drug-induced liver injury (DILI) during the clinical trials, which were previously reported safe during the *in vivo* testing. Additionally, as a vital organ, hepatic cells are always vulnerable to several endogenous and exogenous chemicals and factors that may interfere with the test compound results.[20] It is also challenging to study the vigorously metabolic biological processes with the in vivo liver models.

These facts paved the way to develop a steady *in vitro* model for the liver for a thorough investigation of hepatic pathophysiological mechanisms and the invention of pharmaceutics for hepatic anomalies. Several *in vitro* models are established based on traditional cell culture models consisting of primary human, mouse, and immortal cell lines.[21] However, such models have limited translational capacity, as the liver is a highly vascular organ with a dynamic microenvironment. In contrast, the traditional cell culture

models are static in fluidics. Therefore, they lack the shear stress required for hepatic cells' optimum growth, differentiation, and physiological functions. These limitations of traditional in vitro cell culture models pave the way for the microfluidic-based liver-on-chip (LOC) models.[22] The liver is one of the most common targets of researchers for applying OOC technology. Several liver-on-chip models have been introduced which covered the various anatomical components of a mammalian liver (e.g., hepatic lobule, hepatic acinus) for disease modeling (e.g., non-alcoholic fatty liver disease, fibrosis, carcinomas, viral hepatitis, and drug-induced liver injury) and drug testing (safety, efficacy, and toxicity).[23, 24]

3. Background

3.1. Real-Time Monitoring of Liver-on-Chip

Liver-on-chip (LOC) models contain micro bioreactors, which usually consists of fluidic chambers where liver-specific cells (e.g., hepatocytes, stellate cells, Kupffer cells, microvascular endothelial cells) are cultured on scaffolds, porous membrane, or on a planar surface with the help of liver-specific ECM (e.g., fibronectin, collage).[25] It is essential to examine the metabolic activity and paracellular or intracellular microenvironment of the cells housed in LOC. These factors contribute to several biological phenomena: cell signaling, differentiation, propagation, drug interaction, and cellular metabolism.[26] In the field of *in vitro* pharmaceutical toxicology, potential biohazardous substances are treated with cell cultures, and various biomarkers quantification methods or staining procedures are applied to gauge the impact of the biohazardous substance. LOCs are no exceptions, and traditional biological assays are also being used to study the effect of various types of drugs and biological stimuli.[27] These assays are usually performed at the end of the biological experiment and are called endpoint assays. Endpoint assays only

present the pathophysiological condition of the cells at the end of the experiments. They do not offer the actual time base events causing an injury to the cells. In contrast, the most crucial process for examining the toxicity of a substance is tracing the highly mobile and dynamic state of cellular metabolism.[28] Therefore, the actual overview can only be obtained by consistently tracking the cellular culture microenvironment and not measuring the endpoint assays. A preeminent portion of this overview is the evaluation of the cardinal cell-cell tight junction genesis. The continuous recording of this event permits the evaluation of drug-induced cellular injury and can forecast the pk/pd on the cell or organ level.[29] This provides the basis for the need for real-time monitoring of the LOC devices.

Table 3-1. Liver-on-chip models comparative analysis

Sr. No.	Material	Real-Time Monitoring	Sensors	Sensor Type	ECM	Reference
1	PDMS	Yes	ROS	Fluorescence	Collagen	[30]
2	Glass	Yes	ROS, DO	Fluorescence	Collagen, Porcine Fibronectin	[31]
3	PDMS	Yes	ROS	Fluorescence	Collagen, Fibronectin	[32]
4	PDMS	No	No	-	Collagen	[33]
5	PDMS	No	No	-	Collagen	[34]
6	PDMS	Yes	ROS	Fluorescence	Collagen	[35]
7	PDMS, Glass	No	No	-	-	[36]
8	PDMS	No	No	-	Collagen, Fibronectin, Laminin	[37]
9	PDMS	Yes	ROS	Fluorescence	Collagen, Fibronectin, Matrigel	[38]
10	Glass	Yes	Albumin	Aptamer	Collagen	[39]

4. Material and Methods

4.1. Liver-on-Chip Device Fabrication

The LOC consisted of two major components: two microfluidic glass chips (top and bottom) and a holding gadget to house the glass chips. The glass chips were 101mm thick, 56mm in length, and 41mm in width. While polydimethylsiloxane (PDMS) was used to fabricate anti-leak gaskets. The microfluidic channels were printed on the top glass chips with the help of a 3D inkjet printer by utilizing a medical-grade silicone elastomer (NuSil, Catalogue Number MED-6033) (Figure 4-1). The height of the channel was 300 µm, while the width was set at 800 µm. The holding gadget was also printed by employing the 3D printer. The reason behind preferring soda-lime glass over the traditional PDMS was the non-permeation of the biological molecules and drugs.

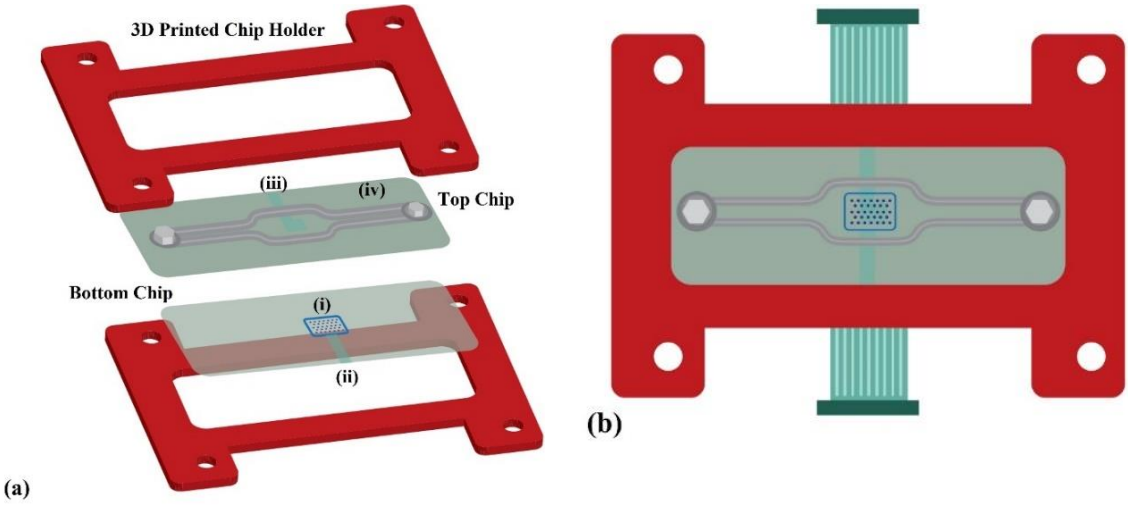

Figure 4-1. The microfluidic glass chip and 3D printer chip holder. **(a)** Open view of the LOC device presenting the ITO based TEER sensor electrodes, while (i) cell seeding & cell culture area (ii) ITO electrode (iii) ITO electrode (iv) microfluidic channel; **(b)** Closed microfluidic chips with 3D printed microfluidic glass chip holder

4.2. Liver-on-Chip Cell Seeding and Tissue Formation

Immortal hepatocyte cell line (HepG2) and immortal human fibroblasts cell line (Hs68) were purchased from Korea Cell Line Bank, South Korea. The cells were grown and propagated in either DMEM media (Dulbecco's Modified Eagle Medium for Cell Culture, Catalogue Number 11965092, ThermoFisher Scientific, USA) or Roswell Park Memorial Institute (RPMI) 1640 cell culture media (Catalogue Number 11875093, ThermoFisher Scientific, USA). The DMEM cell culture media was enriched with 10% fetal bovine serum or FBS v/v (Catalogue Number 16000044, ThermoFisher Scientific, USA) and 1% v/v penicillin & streptomycin (P/S) antibiotic solution (Catalogue Number 15070063, ThermoFisher Scientific, USA). The cells were placed in the humidified cell culture incubate (at 37 °C with 5% CO_2) during the cell culture process for optimum growth. Hepatocytes and fibroblasts were expanded for a minimum of three passages before using any further. The cells were washed with Dulbecco's phosphate-buffered saline (DPBS) (Catalogue Number 14190144, ThermoFisher Scientific, USA) solution after warming in a water bath at 37 °C, for removing the cellular wastes products, dead cells, and cellular debris from the cell cultures. The cells were passaged after reaching the confluency of 90%. A trypsin solution, 0.05% trypsin-EDTA solution (Catalogue Number 253000054, ThermoFisher Scientific, USA), was used for this purpose. Cells were collected, washed, and centrifuged at 3000 rpm for 5 minutes. A cell pellet of defined shape was obtained during this process and was suspended in 1 mL of DMEM cell culture media for cell counting and cell viability assessment. Meanwhile, the microfluidic glass chips were sterilized before cell seeding. All the microfluidic glass chips were disinfected thrice with 95% isopropyl alcohol and then irradiated with UV light for 1 hour inside a biosafety cabinet. A custom build cell seeding, and ECM application kit were developed in-house.

The bottom glass chips were fixed in the cell seeding, and ECM application kits and ECM solutions were applied to facilitate the cells' adherence to the microfluidic glass chip surface. Collagen Type I (Rat Tail) (Catalogue Number C3867-1VL, Sigma Aldrich, Republic of Korea), Poly-L-Lysine (Catalogue Number 0403, ScienCell, USA), fibronectin (Catalogue Number 330100108, ThermoFisher Scientific, USA) were used in the working concentrations of 200 µg/mL, 5 µg/mL and 25 µg/mL respectively. Collagen and fibronectin solutions were prepared in DPBS, while Poly-L-Lysine solution was prepared in triple distilled water. The ECM solution was applied in the quantity of 400 µL to the cell culture or cell seeding area of the microfluidic glass chip by employing the cell seeding and ECM application kit. The microfluidic glass chips were then incubated at 4 °C for 8 hours or overnight. After the overnight incubation of the microfluidic glass chips with ECM solutions, the cell seeding area of the microfluidic glass chips was rinsed with cold PBS, and the cell suspensions were applied. The LOC microfluidic chips were seeded with 1.5×10^5 cells mL^{-1}, while for creating liver fibrosis disease model, hepatocytes and fibroblasts were seeded with 1.5×10^5 cells mL^{-1} at the ratio of 1:8. The chips were incubated overnight in a cell culture incubator before any further application. After the overnight incubation of the microfluidic glass chips were removed from the cell culture incubator and were placed in the chip holding gadget. The microfluidic glass chips were placed in the in-house developed microfluidic platform to form a compact tissue in a dynamic cell culture microenvironment. The in-house developed microfluidic platform has consisted of micro tubbing, bubble trap, cell culture media reservoir (5mL) peristaltic pump, senores, and a controlling device for maintaining the temperature (37 °C ± 0.5 °C) and CO_2 (5% ± 0.1%) concentration as shown in Figure 4-2. The peristaltic pump was operated at

60 µL/min speed to create the shear stress of 0.5 dyn cm^{-2}. The shear stress for the microfluidic glass chip was estimated by employing the following equation.

$$T = 6\mu Q / wh^2$$

Whereas "µ" stands for the viscosity of the fluid or cell culture media, "Q" signifies the rate of the fluid flow or cell culture media, "w" is denoted for the width of the microfluidic channel and "h" represents the height of the microfluidic channel.

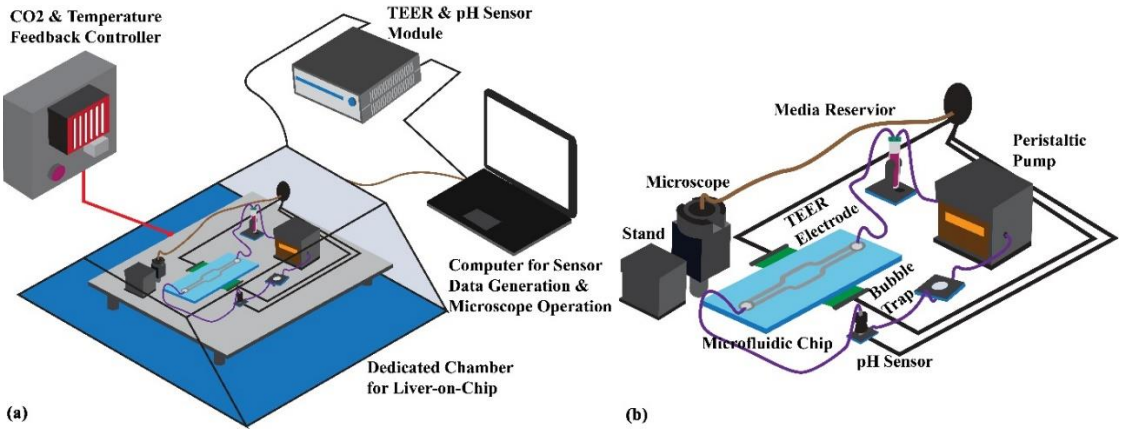

Figure 4-2. (a) Liver-on-chip device platform; **(b)** Liver-on-chip device and accessory components.

4.3. Liver Fibrosis-on-Chip Disease Modeling

Liver fibrosis-on-chip disease modeling was performed by inducing the activation of fibroblasts in the LOC device. Transforming growth factor-beta 1 (TFG-β1) (Catalogue Number ab 50036, Abcam, USA) was utilized for this purpose. TFG-β1 was used at a 5 ng/mL concentration and perfused with the cell culture media for creating a liver fibrosis-on-chip model. The microfluidic based organ-on-chip platform employed for creating a liver fibrosis-on-chip model using LOC device has been shown in the Figure 4-3. Different components of the LOC device and associated electrical hardware is shown in Figure 4-3

(b). While the Figure 4-3 (a) explains the fibrosis inducing mechanism used in the LOC device for creating liver fibrosis-on-chip model.

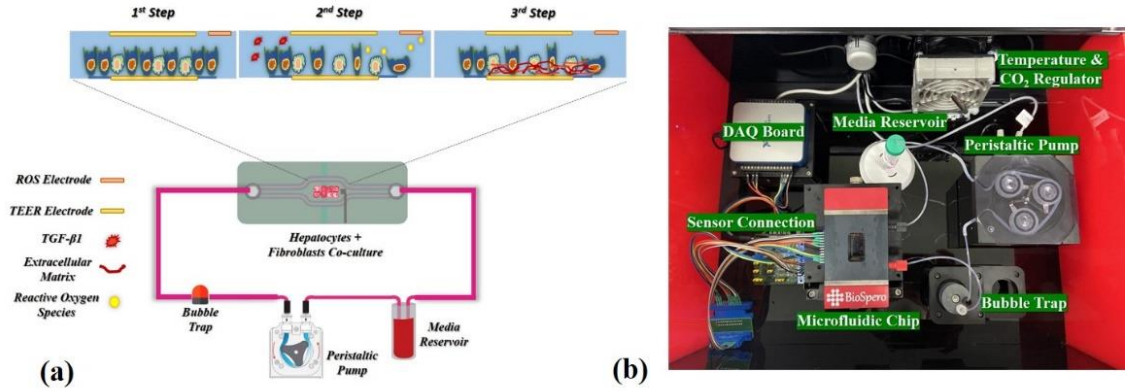

Figure 4-3. (a) The liver fibrosis-on-chip model graphical abstract; **(b)** The real image of liver fibrosis-on-chip model microfluidic system and accessory gadgets

4.4. Drug Concentrations Preparation

Three known anticancer drugs, namely doxorubicin hydrochloride (Catalogue Number A62690, ThermoFisher Scientific, USA), lapatinib (Catalogue Number CDS022971, Sigma Aldrich, Republic of Korea), and epirubicin hydrochloride (Catalogue Number E9406, Sigma Aldrich, Republic of Korea) were utilized in this study. All the drugs were in powder form and weighed with the help of a micro weighing balance (OHAUS Adventurer, Model Number AR2140, OHAUS, USA). Doxorubicin and epirubicin working concentrations were prepared in triple distilled water, while lapatinib working concentrations were formulated in dimethyl sulfoxide (DMSO) (Catalogue Number 472301, Sigma Aldrich, Republic of Korea). Doxorubicin working concentrations were 0.25 µM, 0.50 µM, and 1 µM. At the same time, lapatinib was used in 1 µM, 2 µM, and 5 µM. Epirubicin was applied in the concentrations of 2 µM, 5 µM, and 10 µM.

4.5. TEER, ROS, and pH sensors Development for Real-Time Monitoring

TEER impendence sensor was screen printed by employing the chemical vapor deposition technique (CVD), and 500 nm thick, transparent, indium tin oxide (ITO) electrodes were patterned onto the microfluidic glass chips. The electrodes covered the 16 mm^2 cell culture areas of the microfluidic glass chips, which were overlapping. The impendence was measured by Ω mm^2 using the impendence unit of Ohm (Ω). LabVIEW® was utilized to develop software for the monitoring of the TEER. Similarly, the ROS sensor was also screen printed on the top glass of the microfluidic glass chips by employing a custom-built 3D printer (multi-head). The substrate was cleaned with absolute ethanol, acetone, and double distilled water in the ROS sensor development process. The microfluidic glass chips were then dried and treated with plasma (oxygen) for 15-30 seconds to clean the substrate. Gold (Catalogue Number Au-LT-20 (20 wt%) Fraunhofer, Germany) and silver (Catalogue Number Silver TEC-PA-060, Solvent DA-030, INKtec, South Korea) electrodes were printed at the printing speed of 1 ms^{-1}. After that, sintering was carried out for 15-30 minutes at 130 °C. The characterization of the sensors was carried out by using the PalmSens4 system (Portable, PalmSens, Netherlands), and cyclic voltammetry (CV) was performed using the solutions of potassium ferricyanide ($K_4[Fe(CN)_6]$) (10 mM) and potassium chloride (KCl) (0.1 M). While an in-house developed system took the chronoamperometric response of the sensor. The sensors were rinsed twice with DPBS and triple distilled water for future experiments (Figure 4-4). An optical pH sensor was custom designed using a photodiode, white light-emitting diode, optical filters, and custom-designed assembly (3D printed) (Figure 4-5). The cell culture media usually carries a pH indicator (phenol red) which change sits color due to differences in pH. This phenomenon provides the basis to develop a 3D printed pH sensor. The cell culture media passed through

the transparent microtubing (d= 500 µM) connected with the microfluidic platform's cell culture media reservoir. The pH sensor was calibrated and characterized for a pH range of 6.0-8.5 with several pH samples (cell culture media samples).

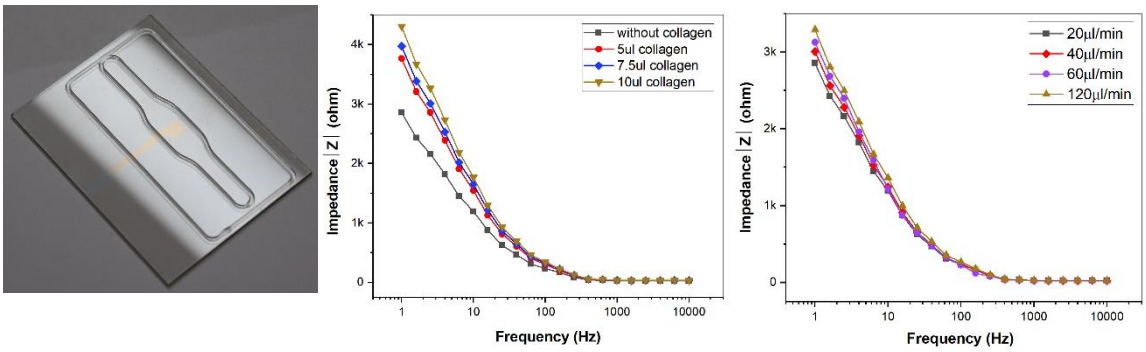

Figure 4-4. (a) Microfluidic glass chip with transparent ITO electrode **(b)** Frequency response of ITO electrodes (TEER sensor) with various concentrations of collagen type I in the absence of cells **(c)** Impendence to frequency data with several flow rates with 5µL collagen type I solution in the absence of the cells.

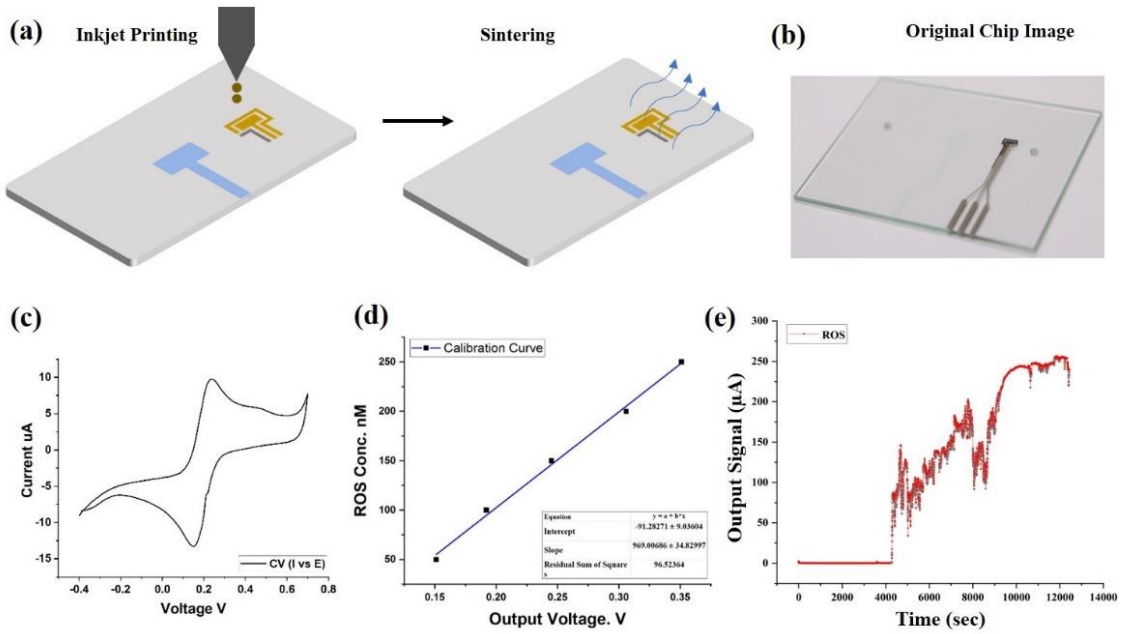

Figure 4-5. The reactive Oxygen Species sensor manufacturing, characterization, and experimental data **(a)** The image shows the fabrication of ROS sensor by inkjet printing and sintering; **(b)** The actual image of the inkjet printer ROS sensor pattern; **(c)** The graph presenting the chronoamperometric response of the ROS sensor by potassium ferricyanide ($K_4[Fe(CN)_6]$) and potassium chloride; **(d)** The graph is showing the data of the calibration curve of the ROS sensor by using several ROS containing solutions at 0.65 V. the data was obtained through the chronoamperometry; **(e)** The graph showing the ROS sensor data of the liver fibrosis-on-chip model. The fibronectin-based liver fibrosis-on-chip model was used for the real-time monitoring of the ROS generation for 14000 seconds or three minutes for each second. The fibronectin-based liver fibrosis-on-chip model produced no ROS until the addition of the TGF-β1 within the LOC device.

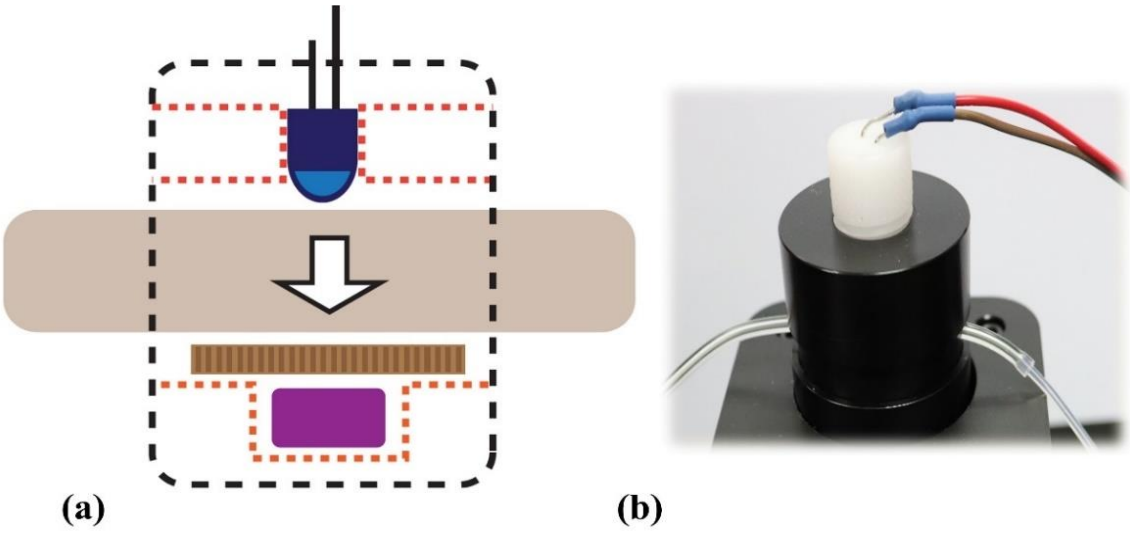

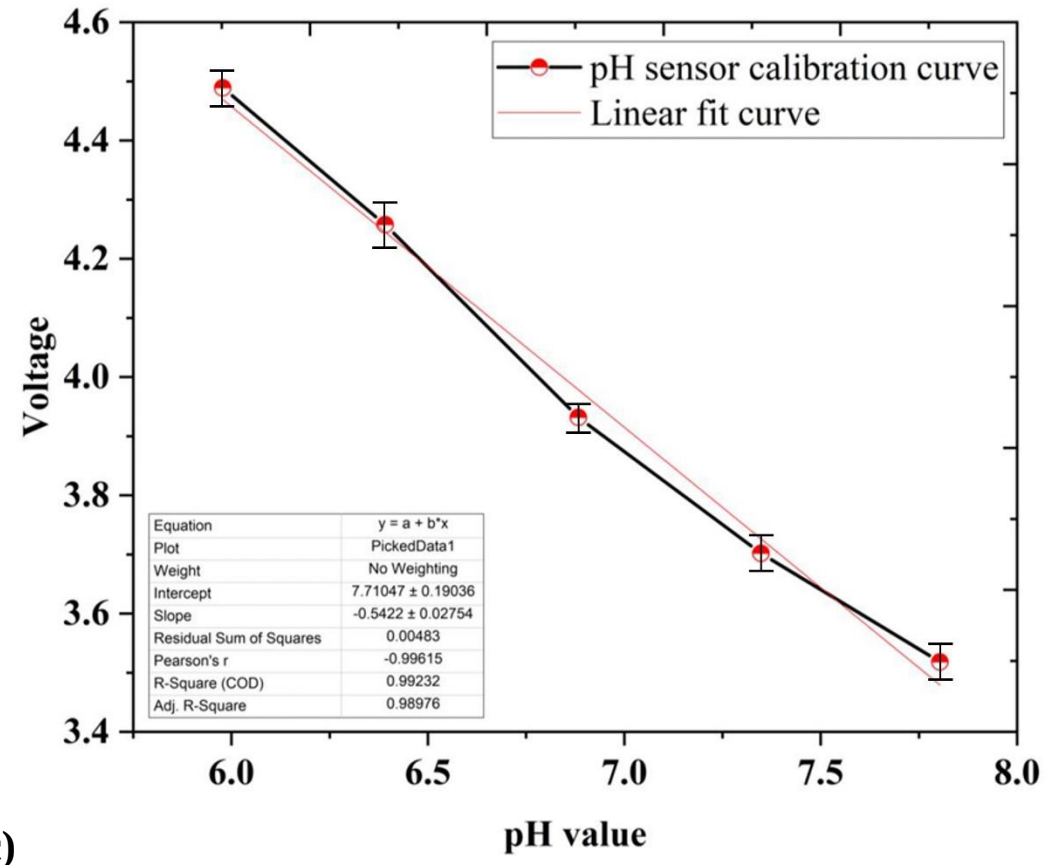

(c)

Figure 4-6. The custom-designed pH sensor **(a)** graphical presentation highlights the principle and different parts of the sensors; **(b)** The actual image of the pH sensor; **(c)** The graph shows the calibration curve data of the custom-designed pH sensor

4.6. Biomarkers Estimation

Albumin, urea, lactate, and CYP450 were measured as the functional biomarkers of the LOC device. The cell culture media samples were collected at different time points and stored at -80 °C for further use. Human Albumin ELISA Kit (Catalogue Number ab108787, Abcam, United States of America), Urea Assay Kit (Catalogue Number KA1652, Abnova, United States of America), Lactate Colorimetric Assay Kit (Catalogue Number K607, BioVision, United States of America), and CYP3A4 Assay Kit (P450-Glo, Catalogue Number V9001, Promega, United States of America) were used to measure albumin, urea,

lactate, and CYP3A4 respectively. Cell culture media samples stored at -80 °C were thawed in a water bath at 37 °C before performing the experiments. The biomarker estimation was performed by following the manufacturer's instructions. The absorbances were taken through a photo spectrometer or a microplate reader (SpectraMax i5 Multimode Microplate Reader, Molecular Devices, United States of America).

4.7. Cell Viability and Immunofluorescent Staining

The live/dead assay was used to determine the cell viability within the LOC. Live/Dead Viability, Cytotoxicity Assay Kit (Catalogue Number L3224, ThermoFisher Scientific, United States of America) was utilized for this purpose. After the termination of the experiments, the cell culture LOC devices were rinsed thrice with pre-warmed DPBA, and then the cell culture area of the LOC device was covered with the live/dead assay reagent (300 µL). The chips were incubated in a cell culture incubator for 30 minutes. After removing the chips from the cell culture incubator, the cell culture area of the microfluidic glass chips was rinsed twice with DPBS. The chips were air-dried at room temperature and mounted with a coverslip by applying the appropriate amount of commercial mounting media. ZO-1, E-cadherin, smooth muscle actin -1 (α-SMA), and collagen immunofluorescence microscopy were performed. Primary antibodies of ZO-1 (Catalogue Number 33-9100, ThermoFisher Scientific, United States of America), Anti-E-cadherin antibody (Catalogue Number ab76055, Abcam, United States of America), α-SMA antibody (Catalogue Number 14-9760-82, ThermoFisher Scientific, United States of America) and collagen type I antibody (Catalogue Number PA1-26204, ThermoFisher Scientific, United States of America) were used for the immunostaining of ZO-1, E-cadherin, α-SMA and collagen type I respectively. While nuclear staining was performed

by using DAPI (Catalogue Number 127M4055V, Sigma-Aldrich, United States of America). In addition to that F(ab)2-goat snit-rabbit IgG (H+L) (Catalogue Number A-21430, ThermoFisher Scientific United States of America), superclonoal^{TM} recombinant secondary antibody (Catalogue Number A28175, ThermoFisher Scientific, United States of America), Alexa flour 488 (Catalogue Number A28175, ThermoFisher Scientific, United States of America) were used as secondary antibodies. The microfluidic glass chips of LOC carrying tissues were rinsed twice with 1x DPBS and fixed with 4% paraformaldehyde to control the tissue's autolysis. While 5% bovine serum albumin (BSA) in DPBS was applied to block the unnecessary building sites within the tissue. Then primary and secondary antibodies were applied and incubated according to the manufacturer's guidelines. After that, chips were washed and mounted with a coverslip for confocal microscopy. A semi-automated confocal laser scanning microscope (Olympus, Model Number FV122, Japan) was employed for taking confocal laser scanning images.

4.8. Fluidic Simulation for Liver-on-Chip Device

The LOC device was simulated by applying the specific configurations through commercial software (ANSYS Fluent).

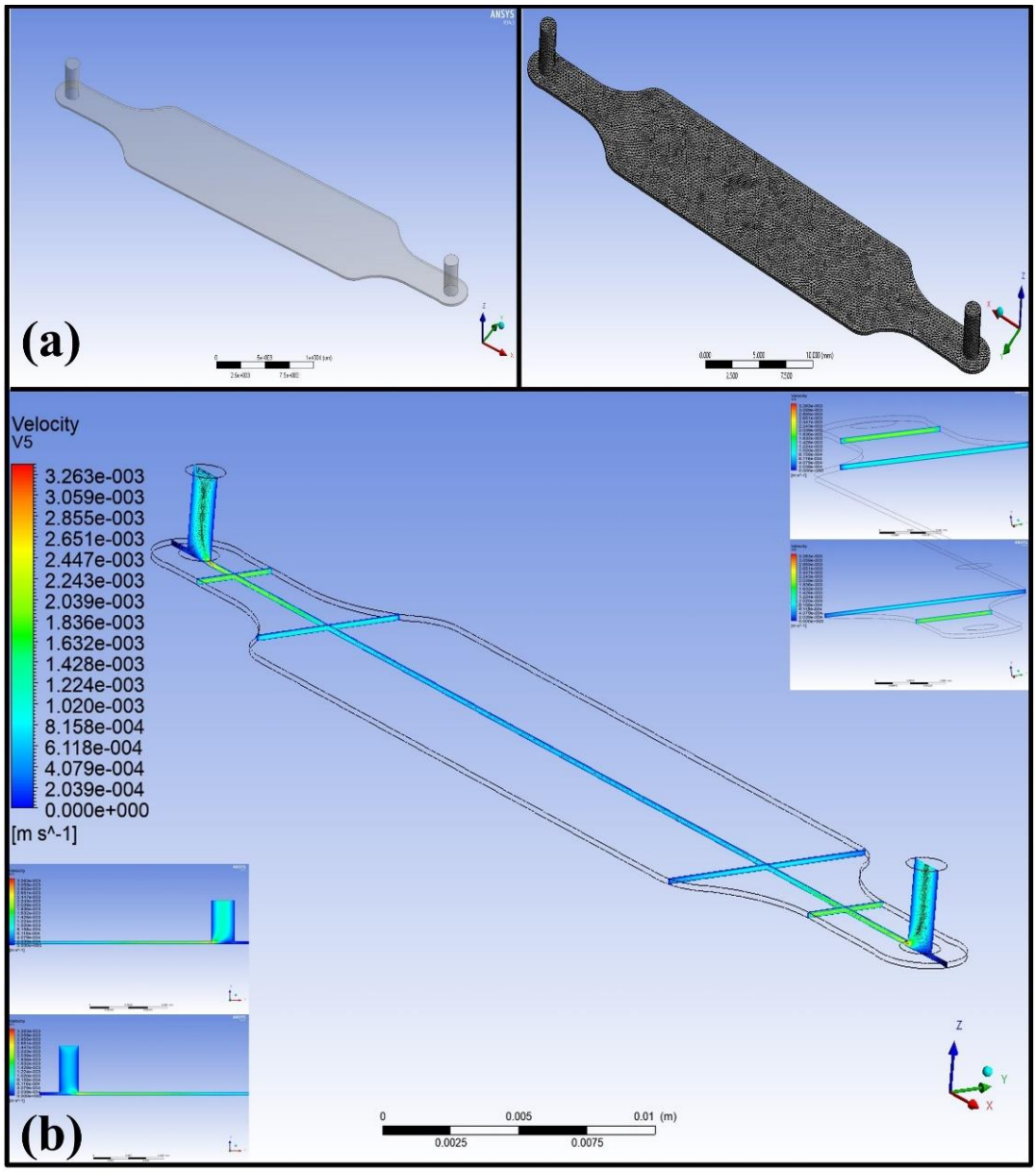

Figure 4-7. The computational simulation of the LOC device; **(a)** The microfluidic channel of the LOC device geometrical design. **(b)** The velocity profiles of the various loci along and across the microfluidic channel. The fluidic dynamic computational simulations of the LOC devices predicted the flow rate of 60 μL min^{-1} and velocity of 0.57 mm sec^{-1} for inducing the shear stress of 0.5 dyn cm^{-2}

5. Results

5.1. Liver-on-Chip Construction and Real-Time Monitoring

The LOC device has been set up as shown in Figure 4-2. The peristaltic pump started feeding the microvolume cell culture media to create shear stress of 0.5 dyn cm^{-2} within the microfluidic chamber of LOC. The real-time monitoring of the LOC device was carried out with the help of an embedded TEER sensor and a non-invasive pH sensor. TEER and pH sensors values based on the sensor responses were taken at 1-hour intervals for 96 hours. The dynamic microenvironment of the LOC device resulted in the hepatocytes' differentiation and propagation, and a compact tissue was formed at 72 hours, as shown in Figure 5-3.

Cellular differentiation and division resulted in replenishing the essential nutritious components of the cell culture media and excretion of metabolic by-products. These cellular excretory materials decreased the pH of cell culture media of the LOC device, and a consistent decrease in the pH of the LOC device was noted under a non-invasive pH sensor. Likewise, TEER sensor data was recorded, and resultant impedance frequency was collected for the LOC (Figure 5-1 (a)). The biological data of impedance vs. frequency (Log_{10}) showed an exponential increase in the TEER values within the LOC. A fixed frequency of 60 Hz was employed to record the TEER sensor data, reflecting a consistent increase in time to impedance. It showed cellular propagation and cell-to-cell tight junction formation among the LOC cell culture area cells. At the same time, the TEER senor was also applied to collect and monitor the TEER impedance values of the static cell culture model. A linear response was noted in the static cell culture model compared to the LOC device with the same type of cells. This phenomenon highlights the significance of a dynamic microenvironment for the cellular culture, which aids cell differentiation and propagation better than static cells.

Similarly, pH senor data from LOC device and static cell culture model showed a decreasing trend in the pH of cell culture media, as shown in Figure 5-1 (b). The LOC device showed a descending ladder-like response, and a lower pH of cell culture media was observed compared to the traditional cell culture model. In contrast, the traditional cell culture model presented a linear decrease in the pH of cell culture media. In parallel, a custom-built 3D microscope was also used to monitor the cell growth in real-time with a 10x optical lens. The custom-built 3D printed microscope was operated with the help of an in-house developed LabView-based software. The micrographs were taken at a working distance of 5.82 mm. The images from a custom-built 3D printed microscope showed a compact hepatic tissue formation on day 3, as shown in Figure 5-3.

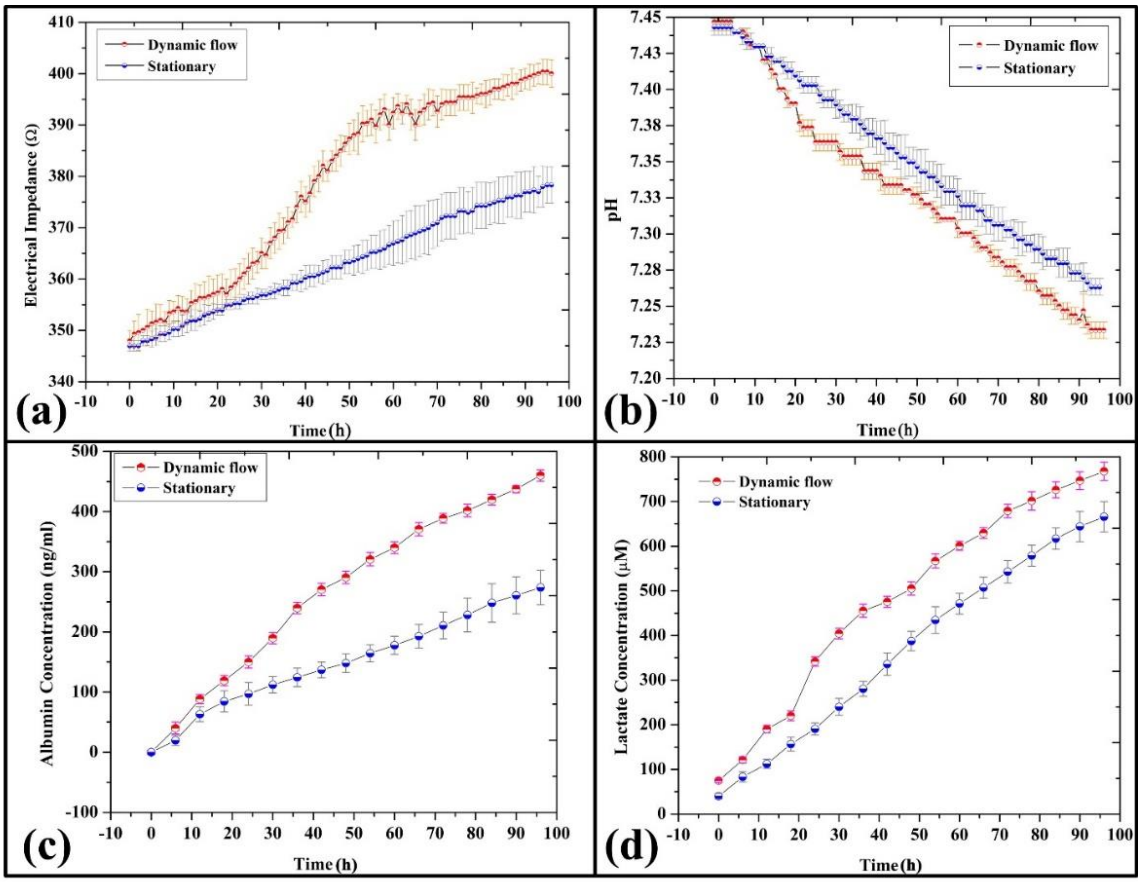

Figure 5-1. (a) The time to electrical impedance graph presents the TEER sensor response of the LOC device. The TEER sensor was applied on the LOC device, and the traditional static cell culture model and TEER values were recorded every hour until 96 hours or three days. The TEER sensor highlighted a consistent increase in the impedance until the 72 hours when the hepatocytes formed a compact hepatic tissue. After that, a slow increase in the TEER was observed compared to before the formation of hepatic tissue. (The data is plotted as mean ± standard deviation while, n=*3*); **(b)** The time to pH graph presents the pH sensor response of the LOC device. The pH sensor was applied on the LOC device, and the traditional static cell culture model and pH values were recorded every hour until 96 hours or three days. The TEER sensor highlighted a consistent decrease in the pH until the termination of the experiment. (The data is plotted as mean ± standard deviation while, n=*3*); **(c)** The graph shows the albumin synthesis by LOC device and the traditional static cell culture model. The albumin synthesis was exponential due to the healthy condition of the hepatocytes present within the LOC device and the traditional static cell culture model. However, the albumin yield by the LOC device was found to be 2-folds more than the traditional static cell culture model. (The data is plotted as mean ± standard deviation while, n=*3*); **(d)** The graph is showing the lactate release by LOC device, and the traditional static cell culture model. The lactate release was found to be exponential due to the healthy metabolic state of the hepatocytes present within the LOC device and the traditional static cell culture model. However, the lactate release by the LOC device was found to be 1-folds more than the traditional static cell culture model. (The data is plotted as mean ± standard deviation while, n=*3*)

5.2. Liver-on-Chip Functional Validation Through Biomarkers

The LOC device functionality was further validated through conventional end-point-based biomarker analysis assays. Albumin is the critical biomarker of hepatocyte pathophysiology, and its production reflects the physiochemical condition of the hepatic

tissue. Hence, cell culture media samples were collected every 6 hours until 96 hours for the LOC device and static cell culture model. An exponential increase was noted in the amount of albumin secreted by the hepatocytes in the cell culture media of the LOC device and static cell culture model (Figure 5-1 (c)). However, a significant difference was noted among the albumin secretion between LOC device and static cell culture model.

Similarly, lactate release is the reflection of glucose metabolism by highly metabolic cells such as hepatocytes. Hence, lactate was quantified to gauge and compare the metabolic activity of the LOC device and static cell culture model (Figure 5-1 (d)). The lactate release followed the pattern found in albumin synthesis, and a consistent increase was observed in lactate release. Likewise, albumin the lactate release was found significantly more in LOC device than the static cell culture model.

TEER reflects the highly mobile and vibrant cellular state, and the cell-to-cell tight junction formation is one of its unique features. Tight junction proteins are a group of transcellular proteins between the cells, present in paracellular spaces and participate in cell division, propagation, locomotion, and metastasis. Hence, E-cadherin (one of the most widely found tight junction proteins in the epithelial cells) expression was studied for the LOC device to validate the TEER sensor data. Additionally, E-cadherin is one of the most abundant cell-to-cell tight junction proteins in hepatic cells. Therefore, the immunofluorescent expression of E-cadherin was found following the TEER sensor data, as shown in Figure 4-2. Furthermore, the expression of E-cadherin increased over time within the hepatic tissue present in the LOC device. The E-cadherin analysis was performed at 24, 48, and 72 hours, respectively, for the LOC device. The micrograph at 24 hours showed the lowest E-cadherin expression than the micrographs collected at 48 and 72 hours. These findings

signified and validated the TEER data, which was kept increasing during the cell culture of hepatocytes within the LOC device. Hence, TEER readings can be served as a substitute for conventional immunofluorescent stating for the cell-to-cell tight junction proteins.

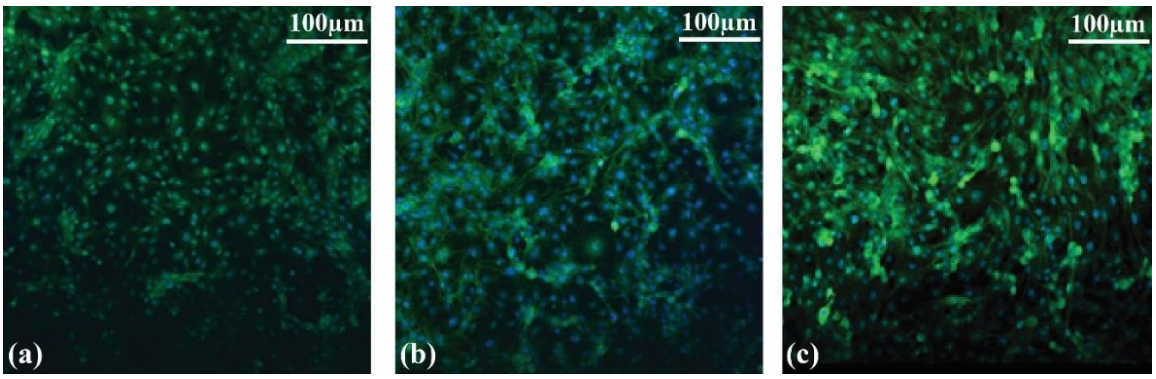

Figure 5-2. The tight junction protein (E-cadherin) expression of LOC device **(a)** LOC device confocal immunofluorescent micrograph taken after 1 day of dynamic cell culture. The green fluorescence depicts the tight junction protein expression; **(b)** LOC device confocal immunofluorescent micrograph taken at day 2 of dynamic cell culture. The expression of tight junction protein (E-cadherin) increased as compared to the expression of tight junction protein (E-cadherin) from day 1; **(c)** LOC device confocal immunofluorescent micrograph taken at day 3 of dynamic cell culture. In addition, the expression of tight junction protein (E-cadherin) increased compared to the expression of tight junction protein (E-cadherin) from day 2.

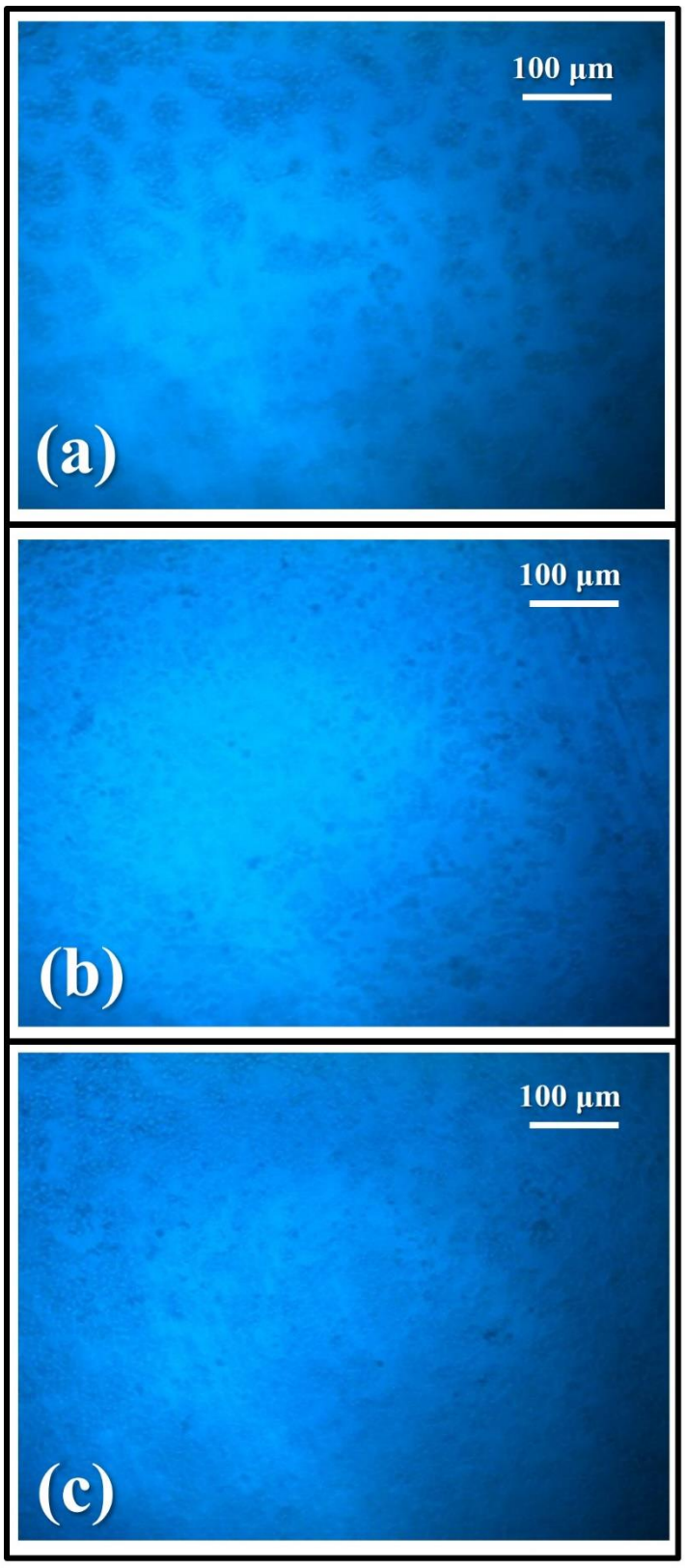

Figure 5-3. Microscopic images were captured by the custom-built 3D printed portable digital microscope through the transparent ITO-based TEER electrode within the LOC device. **(a)** At 24hours of media flow, cells were scattered throughout the cell culture seeding area of the LOC device. **(b)** The cellular confluency increased after 48hours of LOC device function. (c) The resident hepatocytes of the LOC device expanded, eventually covered the whole cell culture seeding area, and formed a characteristic cell monolayer.

5.3. Liver-on-Chip Anticancer Drugs Toxicity Testing

The chip-embedded TEER sensor and non-invasive pH sensor were employed for the LOC device to study the drug toxicity of three known anticancer drugs: doxorubicin, lapatinib, and epirubicin. Several concentrations of the drugs were prepared and perfused with the cell culture media via the reservoir of the microfluidic platform. Minimum four LOC devices were set up at a single time for the drug toxicity evaluation. At the same time, control experiments were performed with drug vehicles (DMSO) and without drugs. All LOC devices were first monitored for 72 hours or until a compact hepatic tissue was formed and the sensors' responses were collected (Figures 5-4, 5-5, 5-6, 5-7). After that, three LOC devices were treated with different concentrations of the single drug, while one LOC device served as the control device.

The embedded TEER senor and noninvasive pH sensor response was further monitored for 24 hours to evaluate the drug toxicity on the resident hepatocyte of the LOC device after treating with known drug doses. In the case of TEER senor response, all the drugs significantly reduced the TEER impendence. It reflects the cell-to-cell tight junction disruption and cellular death due to toxicity induced by the drugs. Doxorubicin in 1μM

concentration was the most toxic drug compared to other drugs Figure 4-6). In contrast, 0.25 µM doxorubicin was the least toxic drug concentration compared to other drugs and their concentrations. Epirubicin and lapatinib had a lesser impact on the TEER as compared to the doxorubicin. However, the toxicity of 5 µM lapatinib was found close to the 0.25 µM doxorubicin. Similarly, the TEER sensor response to 2 µM epirubicin was found nearly like 0.25 µM doxorubicin.

Similarly, pH sensor data also showed a swift drop in the pH of cell culture media after drug treatment for toxicity testing. The lowest pH was observed after the LOC device treatment with 1µM doxorubicin. The difference in pH between 1µM doxorubicin drug dose and the second most toxic drug dose of 0.5 µM doxorubicin was 2-fold lower than all other drug doses. Interestingly, the drug that had the minimum impact on the LOC device's pH of cell culture media was 1µM lapatinib which was not under TEER sensor data. The pH of the cell culture media of the untreated or control LOC device was 7.25.

In contrast, the minimum pH value recorded with the pH sensors during drug toxicity was 6.65. The drugs also significantly influenced the albumin synthesis and lactate release of the hepatocyte biomarker yield and metabolic activity. The normalized lactate and albumin concentrations are shown in Figures 5-8 and 5-9, respectively.

Additionally, live/dead assay was performed to evaluate the cell viability and its relationship with sensors response and biomarker expressions. A relative comparison of cell viability was also carried out based on impedance-based cell viability. The TEER impendence response (normalized) was shown as CI, when they were grown for 72 hours without the drug treatment within the LOC device. The cell index was calculated as flowing

$$\text{Relative Cell Index (CI)} = |Z|_t - |Z|_0 / |Z|_{max} - |Z|_0$$

Whereas $|Z|_t$ is the magnitude of the impedance at the time t. In contrast, $|Z|_{max}$ is the impedance (maximum) noted until the compound (drug) was treated, and $|Z|_0$ is the impedance (lowest) observed until the compound (drug) was treated.

The TEER sensor's impedance-based cell viability estimation was further validated by comparing the results with live/dead assay-based cell viability. TEER senor cell viability was plotted in real-time. In contrast, the live/dead assay-based viability was evaluated at the termination of the experiments after treating with different concentrations of the cytotoxic drugs. The comparative results of impedimetric-based cell viability and live/dead assay-based cellular viability have been shown in Figure 5-10. Doxorubicin (1 µM) was the most toxic dose compared to all other drug doses. In comparison, a slight difference between impedimetric-based cell viability and live/dead assay-based cellular viability was found.

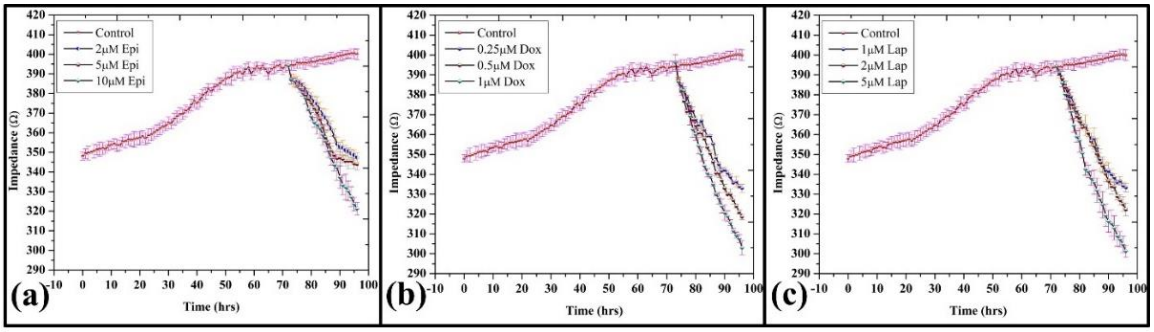

Figure 5-4. The TEER sensor data of cytotoxic drugs (epirubicin. doxorubicin, lapatinib); **(a)** The TEER sensor graph of epirubicin (impedance to time). The TEER sensor responses were taken in Ωmm^2 after every 1 hour. The data was collected for 4 days. During the first three days, the TEER increased due to the cellular expansion and tight junction protein connections and, ultimately, compact hepatic tissue formation. At the start of the day, 4 different drug concentrations (2 µM, 5 µM, 10 µM) were introduced within the LOC via cell culture media

reservoir. The TEER sensor response was further evaluated for another 24 hours. A significant drop in TEER was observed after the drug treatment due to the cellular death and cell-to-cell tight junctions' disruption. (The data presented as ± standard deviation, while the number of the experiment was 3); **(b)** The TEER sensor graph of doxorubicin (impedance to time). The TEER sensor responses were taken in Ωmm^2 after every 1 hour. The data was collected for 4 days. During the first three days, the TEER increased due to the cellular expansion and tight junction protein connections and ultimately the formation of a compact hepatic tissue. At the start of day 4, different drug concentrations (0.25 µM, 0.5 µM, 1 µM) were introduced within the LOC via cell culture media reservoir. The TEER sensor response was further evaluated for another 24 hours. A significant drop in TEER was observed after the drug treatment due to the cellular death and cell-to-cell tight junctions' disruption. (The data presented as ± standard deviation, while the number of the experiment was 3); **(c)** The TEER sensor graph of lapatinib (impedance to time). The TEER sensor responses were taken in Ωmm^2 after every 1 hour. The data was collected for 4 days. During the first three days, the TEER increased due to the cellular expansion and tight junction protein connections and ultimately the formation of a compact hepatic tissue. At the start of the day, 4 different drug concentrations (1 µM, 2 µM, 5 µM) were introduced within the LOC via cell culture media reservoir. The TEER sensor response was further evaluated for another 24 hours. A significant drop in TEER was observed after the drug treatment due to the cellular death and cell-to-cell tight junctions' disruption. (The data presented as ± standard deviation, while the number of the experiment was 3)

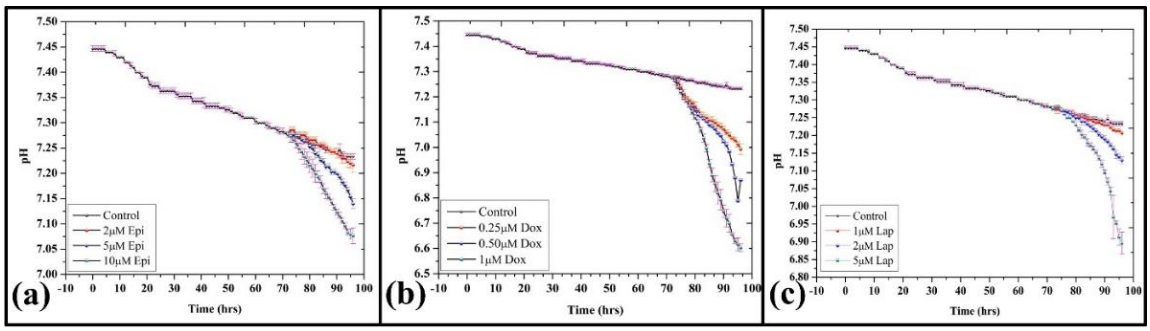

Figure 5-5. The pH sensor was reading against the cytotoxic drugs. The LabView-based in-house developed software was set up to take the pH reading after every one hour. The pH sensor responses were collected for four days. During the first three days, there was no drug treatment, while at the start of the day, four different concentrations of the drugs (epirubicin, doxorubicin, lapatinib) were introduced with the LOC through the cell culture media reservoir; **(a)** The pH sensor data graph is showing the pH change response of the LOC after cytotoxic drug treatment with three different concentrations (2 µM, 5 µM, 10 µM) of the epirubicin. (The data presented as ± standard deviation, while the number of the experiment was 3); **(b)** The pH sensor data graph is showing the pH change response of the LOC after cytotoxic drug treatment with three different concentrations (0.25 µM, 0.50 µM, 1 µM) of the doxorubicin. (The data presented as ± standard deviation, while the number of the experiment was 3); **(c)** The pH sensor data graph is showing the pH change response of the LOC after cytotoxic drug treatment with three different concentrations (1 µM, 2 µM, 5 µM) of the epirubicin. (The data presented as ± standard deviation, while the number of the experiment was 3)

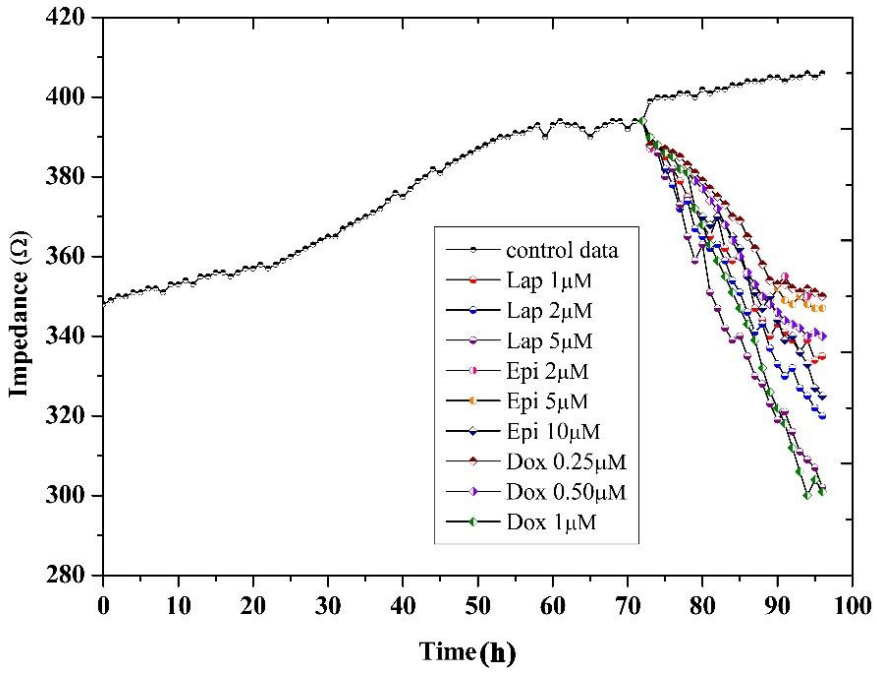

Figure 5-6. The TEER sensor data of LOC devices against cytotoxic drugs (epirubicin. doxorubicin, lapatinib). Several concentrations of cytotoxic drugs have been tested with LOC devices. The TEER sensor was employed for four days. During the first three days, LOC resident hepatocytes expanded, and a cell-cell tight junction formed. At the start of the day, cytotoxic drugs were introduced, and TEER values decreased due to cellular death and cell-cell tight junction disruption. (The data presented as ± standard deviation, while the number of the experiment was 3)

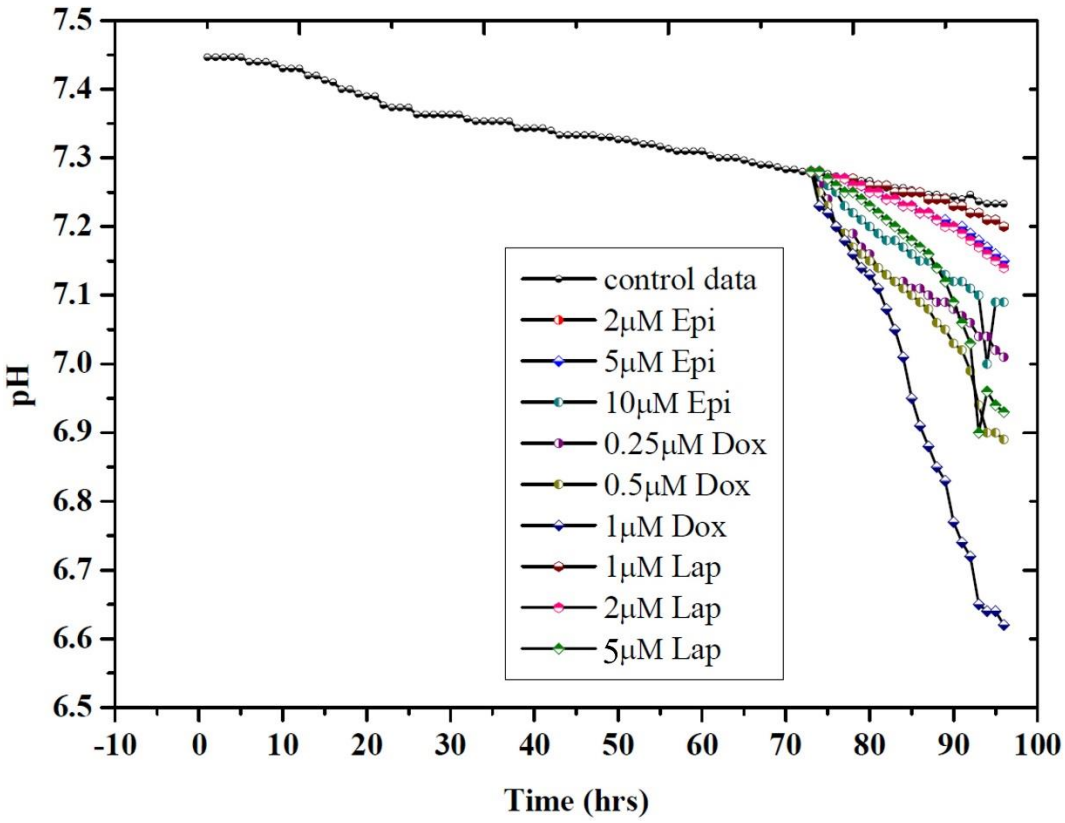

Figure 5-7. The pH sensor was reading against the cytotoxic drugs. The LabView-based in-house developed software was set up to take the pH reading after every one hour. The pH sensor responses were collected for four days. During the first three days, there was no drug treatment, while at the start of the day, four different concentrations of the drugs (epirubicin, doxorubicin, lapatinib) were introduced with the LOC through the cell culture media reservoir. (The data presented as ± standard deviation, while the number of the experiment was 3)

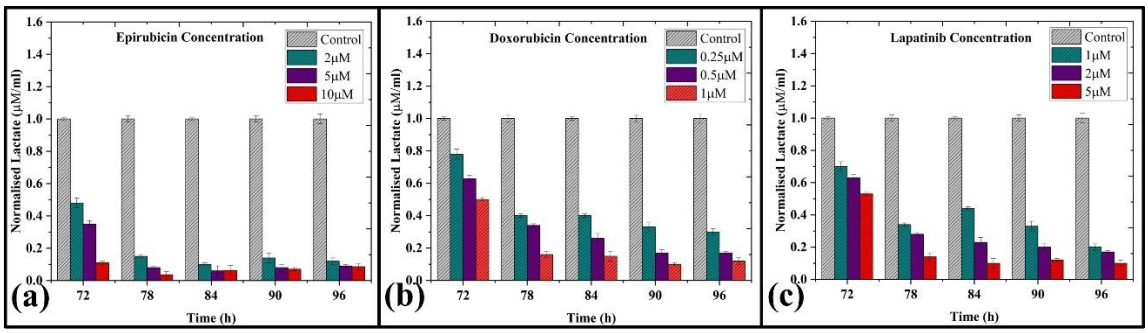

Figure 5-8. The release of lactate from LOC devices after treatment with cytotoxic drugs (epirubicin, doxorubicin, lapatinib) The data was generated after collecting the cell culture media samples from the LOC devices after every six hours (the data presented as ± standard deviation, while the number of the experiment was 3); **(a)** The bar graph is showing the normalized lactate values calculated form the lactate release form the LOC device after drug treatment with different concentrations of epirubicin (2 μM, 5 μM, 10 μM); **(b)** The bar graph is showing the normalized lactate values calculated form the lactate release form the LOC device after drug treatment with different concentrations of doxorubicin (0.25 μM, 0.50 μM, 1 μM); **(c)** The bar graph is showing the normalized lactate values calculated form the lactate release form the LOC device after drug treatment with different concentrations of lapatinib (1 μM, 2 μM, 5 μM)

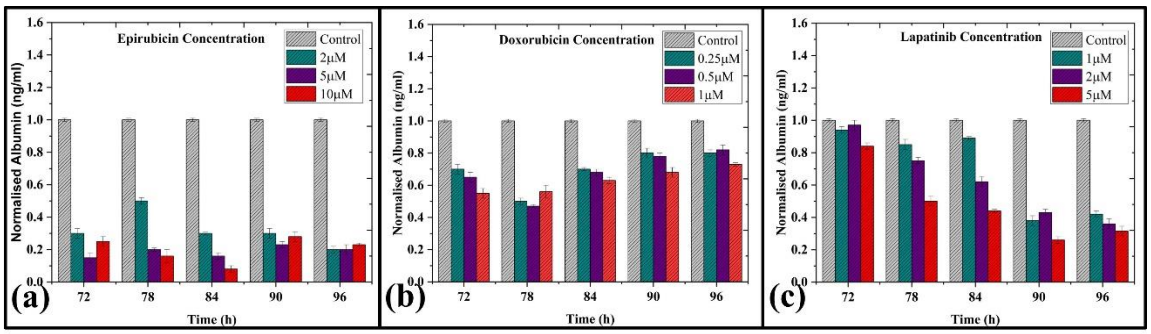

Figure 5-9. The albumin secretion from the resident hepatocytes of LOC devices after treatment with cytotoxic drugs (epirubicin, doxorubicin, lapatinib) The data was generated after collecting the cell culture media samples from the LOC devices after every six hours (the data presented as

± standard deviation, while the number of the experiment was 3); **(a)** The bar graph is showing the normalized albumin values calculated form the albumin synthesis form the LOC device after drug treatment with different concentrations of epirubicin (2 µM, 5 µM, 10 µM); **(b)** The bar graph is showing the normalized albumin values calculated form the albumin synthesis form the LOC device after drug treatment with different concentrations of doxorubicin (0.25 µM, 0.50 µM, 1 µM); **(c)** The bar graph is showing the normalized albumin values calculated form the albumin synthesis form the LOC device after drug treatment with different concentrations of lapatinib (1 µM, 2 µM, 5 µM)

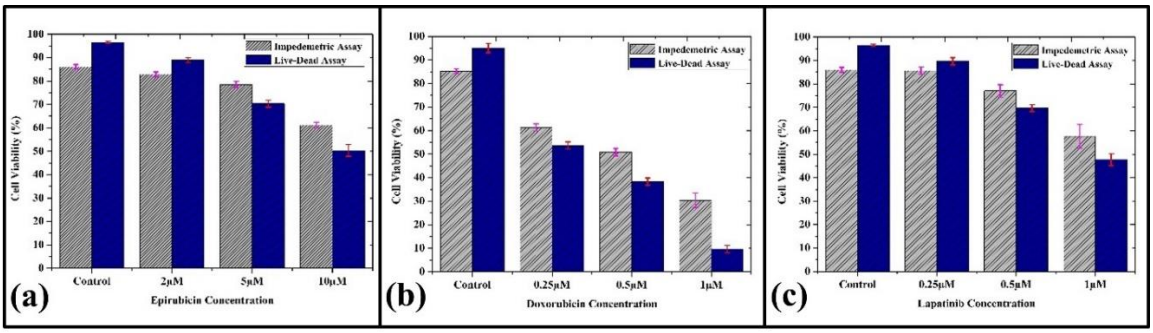

Figure 5-10. The comparative analysis of live/dead assay-based cell viability and impedimteric cell index for different concentration of epirubicin, doxorubicin and lapatinib. hours (the data presented as ± standard deviation, while the number of the experiment was 3)

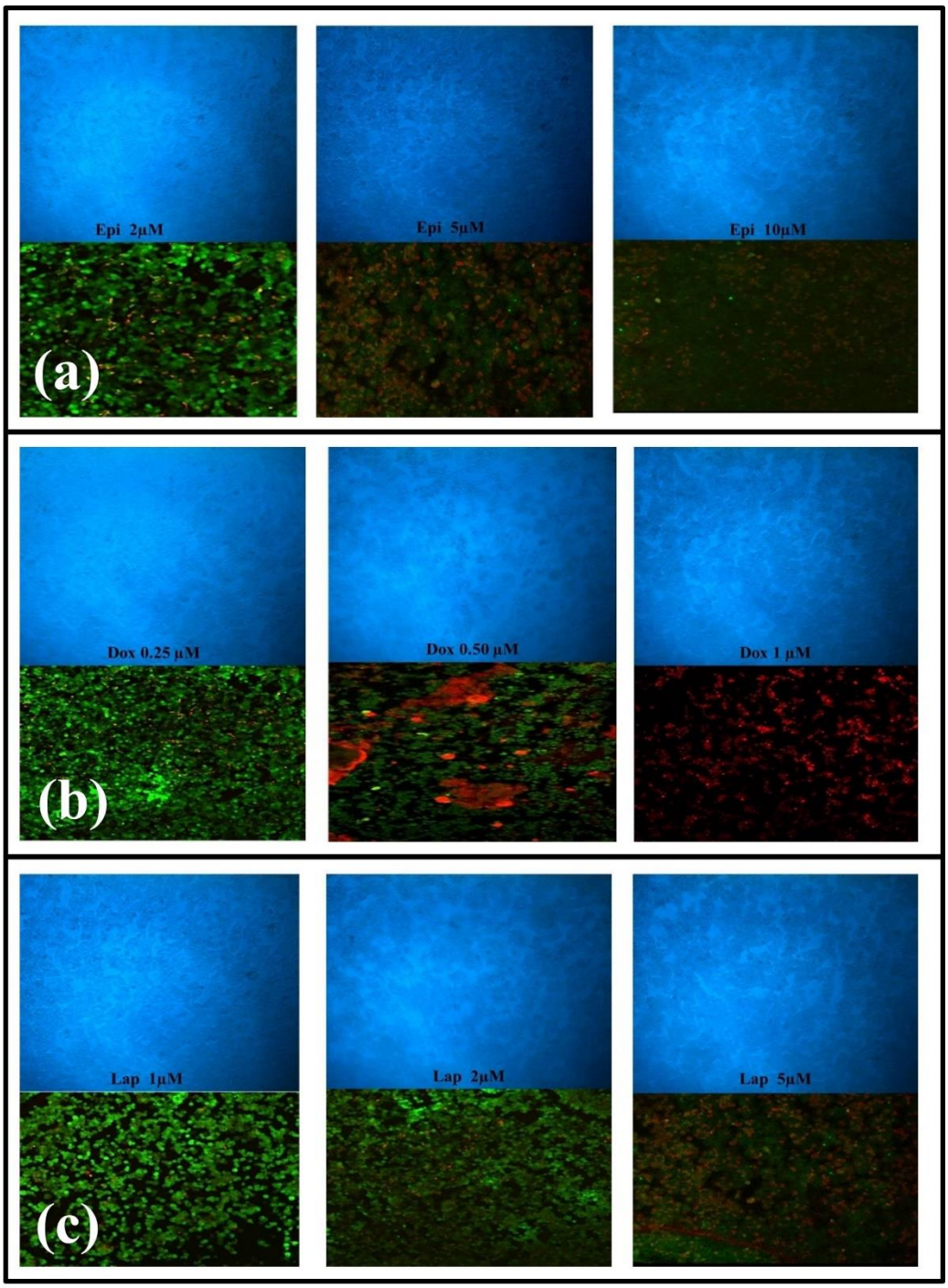

Figure 5-11. Live/dead assay micrographs and the images taken from custom-built (3D Printed) microscope. The micrographs of live/dead assay were processed with ImageJ software. Live and dead cells were counted, and percentage cellular viability was calculated; **(a)** Presenting the micrographs of the LOC device for various cytotoxic concentrations of doxorubicin (0.25 μM,

0.50μM and 1 μM). The cell viability was found as 55%, 40% and 10% respectively. **(b)** Presenting the micrographs of the LOC device for various cytotoxic concentrations of epirubicin (2 μM, 5 μM and 10 μM). The cell viability was found as 90%, 70% and 50% respectively. **(c)** Presenting the micrographs of the LOC device for various cytotoxic concentrations of lapatinib (1 μM, 2 μM, 5 μM). The cell viability was found as 90%, 70% and 50% respectively

5.4. Liver Fibrosis-on-Chip Disease Modeling

The liver fibrosis-on-chip model was developed by co-culturing the hepatocytes and fibroblasts in the ratio of 1:8. The microfluidic platform and associated components have been shown in Figure 3-10. It took three days for the co-cultured cells to form a tissue within the LOC device. A fibrosis-inducing stimulant TGF-β1 in the concentration of 5 ng/mL was introduced within the LOC device through the cell culture media reservoir on the 4^{th} day. The fibrosis-inducing stimulant activated the fibroblast within the LOC device and resulted in the excessive deposition of ECM components. Which is the characteristic feature of hepatic fibrosis.

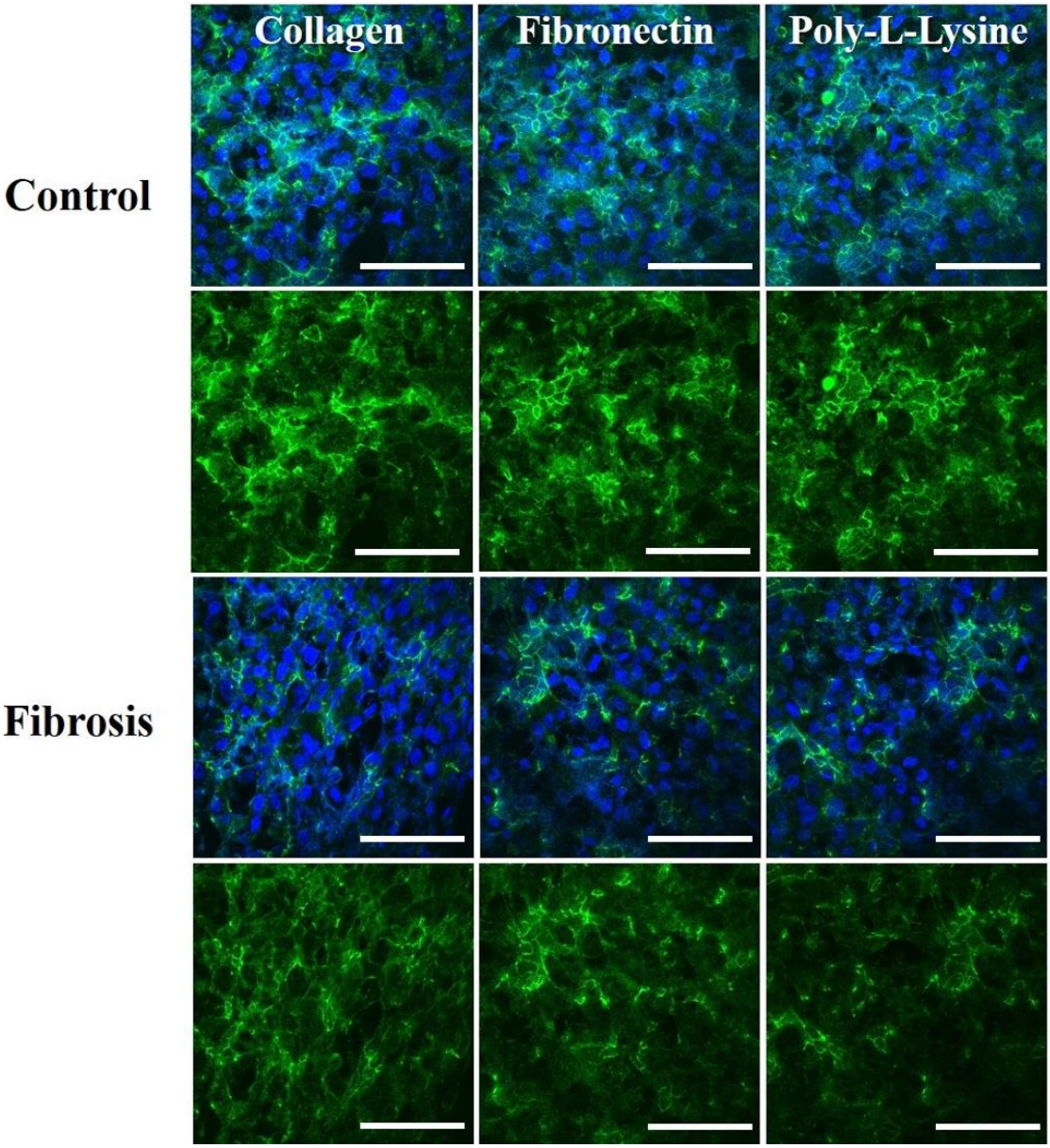

Figure 5-12. Immunofluorescence micrographs show the comparative expression of the liver fibrosis-on-chip model and LOC device's ZO-1(cell-cell tight junction protein) with three different ECM (collagen type I, fibronectin, Poly-L-Lysine). The liver fibrosis-on-chip model was treated with a fibrosis-inducing stimulant, TGF-β1, while the LOC device was used as a control without treating with fibrosis-inducing stimulant TGF-β1. The immunofluorescence micrographs were taken from the tissue samples collected at the end of the experiment on day 6. Whereas white lines represent the scale bar which is 200 µM

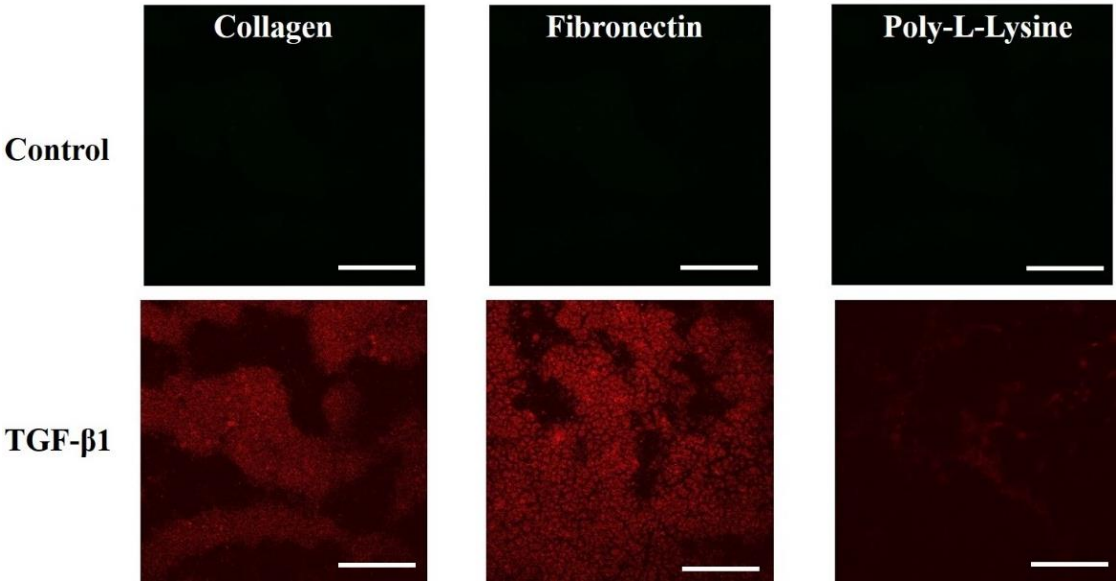

Figure 5-13. Immunofluorescence micrographs show the comparative expression of the resident fibroblasts of the liver fibrosis-on-chip model and LOC device's α-SMA with three different ECM (collagen type I, fibronectin, Poly-L-Lysine). The liver fibrosis-on-chip model was treated with a fibrosis-inducing stimulant, TGF-β1, while the LOC device was used as a control without treating with fibrosis-inducing stimulant TGF-β1. The immunofluorescence micrographs were taken from the tissue samples collected at the end of the experiment on day 6. Whereas white lines represent the scale bar which is 200 µM

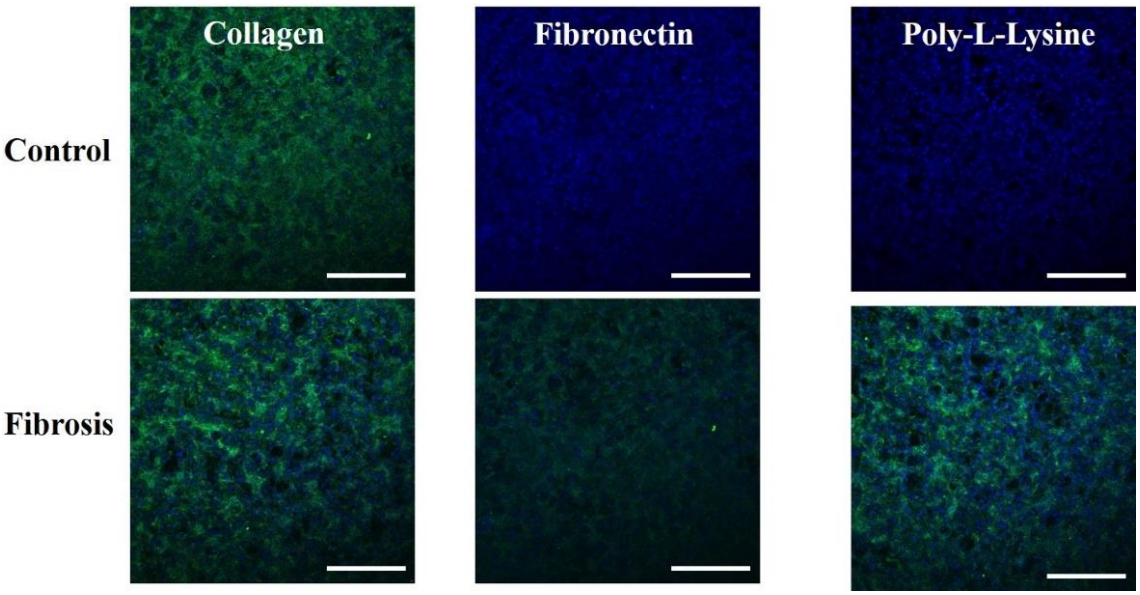

Figure 5-14. Immunofluorescence micrographs show the comparative expression of the liver fibrosis-on-chip model and LOC device's collagen type I with three different ECM (collagen type I, fibronectin, Poly-L-Lysine). The liver fibrosis-on-chip model was treated with a fibrosis-inducing stimulant, TGF-β1, while the LOC device was used as a control without treating with fibrosis-inducing stimulant TGF-β1. The immunofluorescence micrographs were taken from the tissue samples collected at the end of the experiment on day 6. Whereas white lines represent the scale bar which is 200 μM

5.5. Liver Fibrosis Prediction Using TEER Sensor

The liver fibrosis-on-chip disease model was real-time monitored for six days and the and the response of the embedded TEER sensor was collected every one hour. The TEER data showed a consistent increase in the impedance value, which signs the co-culture cells propagation, expansion, and compact tissue formation within the LOC device until the day 3 or 72 hours. At the start of day 4, a fibrosis-inducing stimulant was introduced. The impedance values were found to be the lowest on the 5^{th} day due to the negative impact of TGF-β1 on the LOC device and resulted in the disruption of cell-t-cell tight junctions. After that, an increase in the impedance value was observed. This increase was due to the deposition of ECM components within the liver fibrosis-on-chip model due to the activation of the fibroblasts, as evident from Figure 5-15.

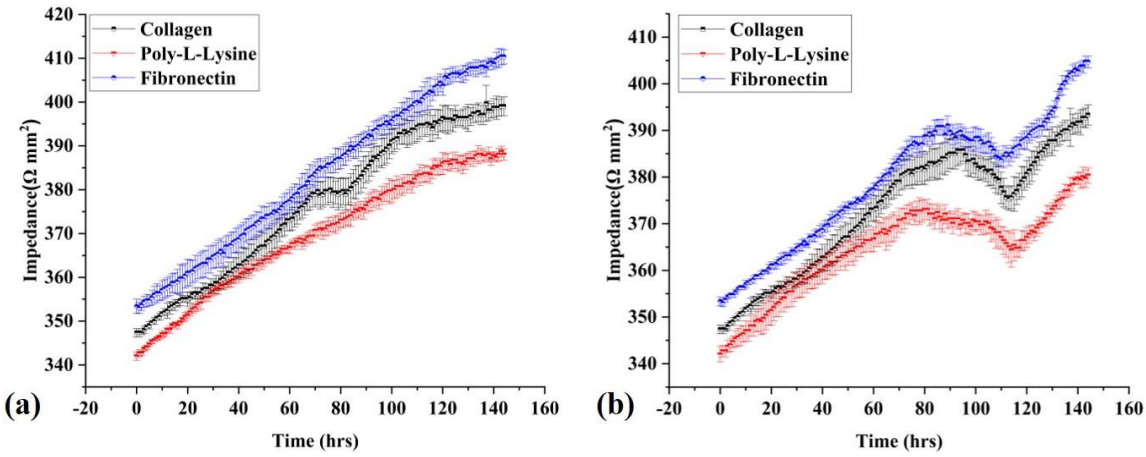

Figure 5-15. TEER sensor data collected in Real-Time **(a)** The graph shows the TEER sensor data collected in Real-Time from LOC devices with different types of extracellular matrix (collagen, Poly-L-Lysine, fibronectin). The data was collected from the LOC devices after every one hour (the data presented as ± standard deviation, while the number of the experiment was 3); **(b)** The graph shows the TEER sensor data collected in Real-Time from liver fibrosis-on-chip model with different types of extracellular matrix (collagen, Poly-L-Lysine, fibronectin). The Liver fibrosis-on-chip model was created after treating with a fibrosis-inducing stimulant, TGF-β1. The hepatocyte and fibroblasts co-culture propagated and expanded until the formation of a compact tissue on day three, and a steady increase in TEER value was observed. The fibrosis-inducing stimulant TGF-β1was introduced within the liver fibrosis-on-chip model at the start of day four. The TEER values started drooping due to the loss of cellular viability. After one day, the TEER value increased again due to fibroblasts' activation and extra deposition of ECM components within the liver fibrosis-on-chip model. The data was collected from the LOC devices after every one hour (the data presented as ± standard deviation, while the number of the experiment was 3)

5.6. Estimation of ROS within Liver Fibrosis-on-Chip Model Using ROS Sensor

A chip embedded ROS senor was employed to study the formation of ROS during the hepatic fibrosis progression. The noninvasive embedded ROS sensor was designed to

quantify the formation of H_2O_2 within the liver fibrosis-on-chip model. The ROS release was monitored for 3 hours within the liver fibrosis-on-chip model. Before the perfusion of fibrosis-inducing stimulant (TGF-β1), the ROS release was monitored, and no significant release of ROS was observed, as shown in Figure 4-4. However, after the introduction of TGF-β1 within the LOC device, a quick release of ROS was observed and for the first minute. A drop in ROS release was noted at the start of the third minute; after that, the ROS release increased.

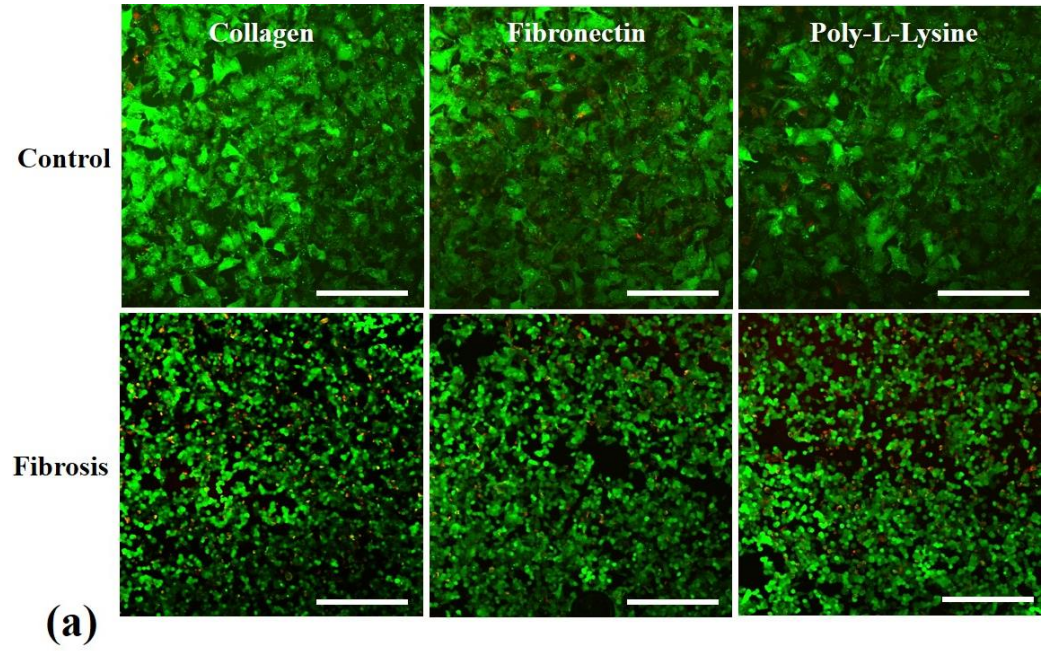

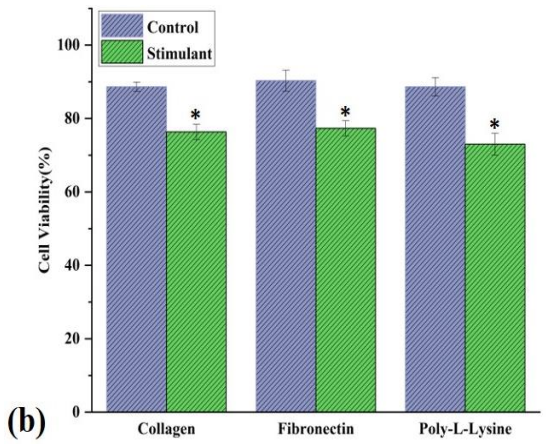

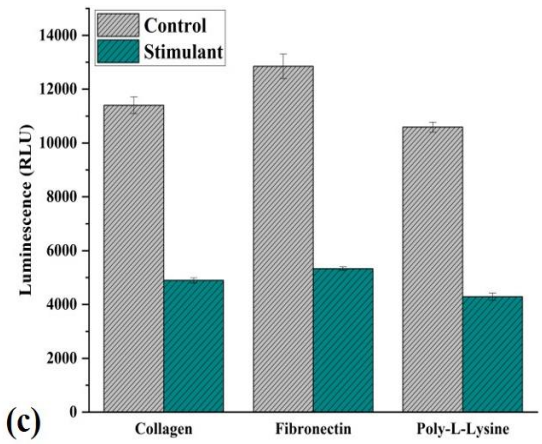

Figure 5-16. (a) The image shows the Live/dead assay micrographs. The live/dead assay micrographs were further processed with ImageJ software to count viable and dead cells. Whereas white lines represent the scale bar 200 µM; **(b)** The bar graph presents the comparative live/dead assay percentage cellular viability of LOC device (control) and liver fibrosis-on-chip model. LOC devices based on fibronectin, collagen, and Poly-L-Lysine showed 90%, 88%, and 88% viability, respectively. In comparison, the liver fibrosis-on-chip model based on fibronectin, collagen, and Poly-L-Lysine showed 77%, 76%, and 73% cellular viability. (The data is shown as mean values ± standard deviation while * is statistical significance from the LOC device (control); **(c)** The bar graphs present the comparative expression of CYP3A4 from LOC device and liver fibrosis-on-chip model **(**The data is shown as mean values ± standard deviation, where the number of experiments is 3)

5.7. Effect of Extracellular Matrix on Liver Fibrosis-on-Chip Model

ECM is one of the allied components of an organ-on-chip construction as it offers and anchors space for cells to settle and propagate or differentiate. The composition of ECM is peculiar to each organ. Hence, several types of ECM are being utilized for organ-on-chip development. The efficiency of three common ECM (collagen, fibronectin, and Poly-L-Lysine) was studied for LOC devices using the chip embedded noninvasive TEER sensor. The TEER sensor response for different ECM has been presented in Figure 5-15. TEER values for fibronectin were found to be higher as compared to fibronectin and Poly-L-Lysine. In contrast, Poly-L-Lysine yielded the minimum TEER response.

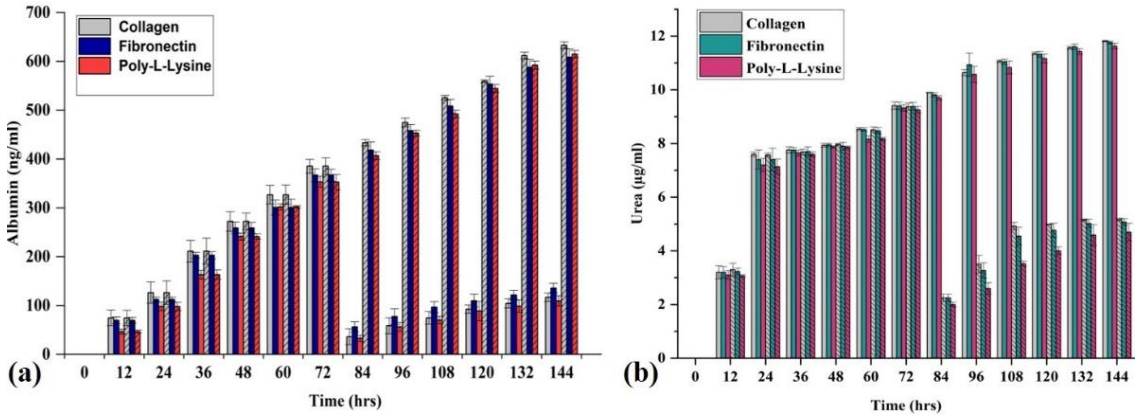

Figure 5-17. (a) The bar graph presents the albumin synthesis by LOC device and liver fibrosis-on-chip model for six days. The albumin release from the resident hepatocytes was significantly decreased after the treatment LOC and liver fibrosis-on-chip model with fibrosis-inducing stimulant TGF-β1. (The data is shown as mean values ± standard deviation, where the number of experiments is 3, while crossbars present the liver fibrosis-on-chip model); **(b)** The bar graph presents the urea release by LOC device and liver fibrosis-on-chip model for six days. The urea release from the resident hepatocytes and fibroblasts significantly decreased after the LOC and liver fibrosis-on-chip model with fibrosis-inducing stimulant TGF-β1. (The data is shown as mean values ± standard deviation, where the number of experiments is 3, while crossbars present the liver fibrosis-on-chip model)

6. Discussion

6.1. Liver-on-Chip Based Drug Toxicity Testing

A LOC device was developed for the real-time motoring of drug toxicity testing. Microfluidic glass chip embedded TEER, non-invasive pH sensor, and custom-built 3D printed compound light microscope were employed to evaluate the impact of toxic drugs on the resident hepatocytes of the LOC. The primary purpose of real-time monitoring technology was to study the biological processes for an extended period without casting any negative effect on the hepatic tissue and LOC device. Traditionally, TEER is measured through the commercial TEER sensor, which usually has invasive probes or electrodes,

and their electrical signal interferes with several types of cells. In addition, the commercial TEER measurement systems are laborious and usually not compatible with organ-on-chip systems. The TEER sensors developed in the current study proposed a TEER range for forming a compact hepatic tissue within the LOC device without interfering or negatively affecting the resident hepatocytes of the LOC device. The TEER range corresponding to the formation of a compact hepatic tissue was 345-395 Ω/mm^2.[40] This range can be served as a reference for culturing the hepatocytes with a glass-based microfluidic LOC device. The complex mammalian tissues also serve as a bioelectrical structure, and their electrical transduction occurs in paracellular and transcellular directions. This electrical transduction depends upon various allied factors such as cell type, ECM composition, tissue thickness, tight junction protein expression, and the pathophysiological role of that particular tissue.[41, 42] The current study evaluated the role of electrical transduction within the paracellular direction or cell-cell tight junction formation.

TEER predicts the pathophysiological state of cell culture; the lower than usual TEER forecasts the unhealthy state of the resident cells of the cell culture while the TEER values within a reference range signify the healthy physiological state of the resident cells or the tissue present in cell culture.[43, 44] The proposed TEER range was also verified with traditional biomarker assays in the current study. Tight junction formation is peculiar to nearly all mammalian cells and to epithelial cells. However, some factors may interfere with the optimum TEER range: cell passage number, type of ECM used, and other nutritional components present within the cell culture media (FBS).[45-48] Previously, it was described that the cell culture environment's temperature negatively affects the TEER of compact tissue.[49]

Other allied factors influence cell culture's pathophysiological condition, and the pH of the cell culture media is one of those. Maintenance of the cell culture media pH is vital to the health of the resident cells of the cell culture. A minor change in the pH range can drastically impact the cell culture.[50] Hence, an in-house developed non-invasive pH sensor was developed for the real-time monitoring of the tissue microenvironment of the LOC device. A physiological pH range (7.45-7.22) was found as the optimum pH range for the hepatocytes culture within the microenvironment of the glass-based LOC device. Certain factors directly alter the pH of the cell culture media and can be exploited as the indicator of pathophysiological events. A swift decrease in the pH of cell culture media highlights the increase of acidic metabolic products by the resident cells of cell culture. The acidic products are usually the result of dead cell debris, infections, and cell toxicants application.[51, 52] The present study found that the cytotoxic drugs result in a steady and swift drop of cell culture media pH, and hence, pH monitoring can be employed as a tool for drug toxicity testing.

The distinction of the microfluidics-based organ-on-chip technology from traditional cell culture systems is the induction of physiological shear stress. Physiological shear stress is one of the most critical factors for optimum cellular growth, propagation, and differentiation.[6, 53, 54] It was found that the hepatocyte from the same passage and origin perform differently in a traditional cell culture model and a LOC device. The LOC device's albumin yield by the resident hepatocytes was found 2 times more than the resident hepatocyte of the traditional cell culture model. These phenomena signify the impact of shear stress on the cell culture. Likewise, lactate release was also found three times more by the resident hepatocytes of the LOC device in comparison with the traditional cell

culture model. Shear stress applied to the cell cultures increased and optimized the cells' biomarker yield and metabolic activity.

In the present study, three commonly used drugs for drug toxicity testing were used to study the impact of drug toxicity on the LOC and the sensor responses. Epirubicin, doxorubicin, and lapatinib were used for this purpose. Epirubicin and doxorubicin are toxic to the genetic material, and they downregulate the intracellular protein synthesis vital for DNA maintenance.[55, 56] As a result, the ROS generated by these two drugs results in the death of the target cell. At the same time, lapatinib downregulates the tyrosine kinase pathways and leads to cellular growth arrest of the cancer cells.[57] The toxicity induced by these drugs was studied with the help of real-time sensors, and cell viability was estimated by live/dead assay and TEER sensor-based impedimetric viability.

Additionally, a biomarker analysis of albumin synthesis and lactate release was performed. The cytotoxic drugs impacted all these parameters and resulted in the decrease of cell viability. The higher the drug concentration, the lower the albumin synthesis was noted. Similarly, the higher drug doses lead to a decrease in the lactate released, showing that the resident hepatocytes are not fully functional due to toxicity. For example, the doxorubicin dose of 1 µM reduced the LOC device's resident hepatocyte viability (10%). In a previous study, the cell viability of hepatocytes was noted as 20% with a 1 µM dose of doxorubicin. The impedimetric cell viability also showed a higher value to the same drug concentration, exhibiting higher cellular death. But it was found lower than the live/dead assay-based viability. It can be attributed to the cell attachment to the ITO sensor surface.

6.2. Real-Time Monitoring of Liver Fibrosis-on-Chip Model

In the subsequent study, the LOC device and embedded senor were used for exploring the possibility of TEER sensor and ROS sensor-based hepatic fibrosis prediction. Here, the resident hepatocytes of the LOC device were cultured with fibroblasts in the ratio of 1:8, which is a physiological ratio of fibroblasts within the human hepatic tissue. The LOC was device was set up and real-time monitored for 6 days. A compact hepatic tissue formation was noted at the end of day three, and a TEER reference value of 370-390 Ω/mm^2 was noted.[40] This TEER range was found to a slightly different from the previous study. This difference can be attributed to the cellular co-culture of hepatocytes and fibroblasts, while only hepatocytes were cultured in the previous study.

Additionally, in the current study, 5% FBS was used in the cell culture media compared to the 10% FBS used in the previously reported study. A fibrous-inducing stimulant TGF-β1 was introduced within the LOC device through the cell culture media reservoir on the 4^{th} day. As a result, the TEER values started dropping due to the subsequent cellular injury and cell-to-cell tight junction disruption. However, at the 95^{th} hour, the TEER values started increasing due to the activation of resident fibroblasts of the LOC device. The activation of fibroblasts resulted in the deposition of excessive ECM within the LOC device, and the TEER sensor accurately detected this change.

At the same time, the ROS sensor detected a swift increase in the release of ROS within the LOC device on the introduction of fibrous-inducing stimulant TGF-β1. However, after 1 hour of the introduction of fibrous-inducing stimulant TGF-β1, the ROS concentration started decreasing. This decrease in ROS concentration can be due to the lower number of viable resident cells. Likewise, the biomarker yield was noted to keep increasing within the LOC device before introducing fibrous-inducing stimulant TGF-β1. However, the

introduction of fibrous-inducing stimulant TGF-β1 resulted in a decrease in biomarker yield. CYP3A4 belongs to the intracellular metabolic enzyme family of CYP450 and is known to participate in the drug molecule catabolism up to 50%. The introduction of fibrous-inducing stimulant TGF-β1greatly reduced the activity of the CYP3A4.[58, 59] However, the overall activity of the CYP3A4 was found one time more than the CYP3A4 activity of the traditional static cell culture model. The CYP3A4 compromised activity can lead to lower drug availability for anti-fibrosis treatment. A previous study found the relationship of fibrous-inducing stimulant TGF-β1 with CYP3A4 lower activity due to the downregulation of the hPXR pathway.[48]

Similarly, the albumin synthesis by the resident hepatocyte of the LOC device decreased four times more than the control LOC device. Tight junction proteins are vital and gatekeepers of cell-t-cell interactions and tissue integrity. The hepatic cell-to-cell tight junction protein was found to be varying in response to the fibrosis-inducing factors. The expression of ZO-1 was found poorly integrated within the LOC device treated with fibrous-inducing stimulant TGF-β1, which can be a reason for the decrease in TEER in the liver fibrosis-on-chip model.[60] In comparison, the expression of ZO-1 was found intact in the control LOC device. α-SMA is an intracellular cytoskeleton and is known to highlight the activation of fibroblasts. A strong expression of α-SMA within the resident fibroblasts of the liver fibrosis-on-chip model was found. At the same time, the control LOC device was found negative for α-SMA.

ECM is an integral part of all types of cell cultures and provides an anchor to the resident cells of the cell culture.[61] The composition of ECM varies from tissue to tissue and may alter during certain pathophysiological conditions. The typical components of ECM are

collagens, fibronectin, fibrinogen, and laminins. There are various studies available on the role of ECM in cell culture.[62, 63] However, the role of ECM for organ-on-chips has not to be studied so far. Different types of ECM were applied to the liver fibrosis-on-chip models to question the role of ECM in liver fibrosis-on-chip models. The cellular viability was found 33% decreased for fibronectin, 24% for collagen, and 27% for poly-L-lysine. The fibronectin was found to be the best ECM type for construction and glass chip-based LOC devices. At the same time, poly-L-lysine and collagen can also be used for this purpose.

7. Conclusion and Future Perspectives

In the present work, a microfluidic glass chip-based LOC device was developed with integrated non-invasive chip embedded and 3D printed sensors. The microfluidic platform was designed to carry out drug toxicity testing and disease modeling. Traditional glass slides were modified, the coating was applied. In addition, a 3D printer was employed to print a microfluidic channel, a custom-made chip holder, and cell seeding kits were used for growing cells on the microfluidic glass chip. Furthermore, ITO electrodes were printed, and a novel TEER sensor was developed. The transparency of the glass chips aided the live microscopy with the help of a 3D printed microscope. The TEER and pH sensor successfully monitored the drug toxicity, and 1μM doxorubicin was the most toxic drug dose for the LOC device. Subsequent biomarker data and confocal leaser microscopy results suggested that the non-invasive TEER and pH sensors can be used with LOC devices for rela0time monitoring and can be an alternative to the traditional bioassay.

In the next step, the LOC device was co-cultured with fibroblasts and hepatocytes, and a fibrosis-inducing stimulant was used to create a liver fibrosis-on-chip model. Here, a 3D printed chip embedded non-invasive ROS sensor was developed and used to study the role of ROS in the liver fibrosis-on-chip model. Finally, various ECMs were evaluated to find the best ECM for the LOC device. TEER sensor data was compared with biomarker results, and it was found that TEER sensor can be applied for studying in vitro heptoic fibrosis models. While ROS sensor successfully monitored the release of ROS with liver fibrosis-on-chip model.

In conclusion, the developed non-invasive TEER, pH, and ROS sensors can be employed for real-time monitoring of organ-on-chip devices and serve as an alternative to traditional

bioassays. However, there is a need to apply these sensors for other organ chips, and their validation can be carried out with molecular biological techniques.

8. References

1. Dittrich, P.S. and A. Manz, *Lab-on-a-chip: microfluidics in drug discovery.* Nature reviews Drug discovery, 2006. **5**(3): p. 210-218.
2. Paoli, R. and J. Samitier, *Mimicking the kidney: A key role in organ-on-chip development.* Micromachines, 2016. **7**(7): p. 126.
3. Zhang, B., et al., *Advances in organ-on-a-chip engineering.* Nature Reviews Materials, 2018. **3**(8): p. 257-278.
4. Jodat, Y.A., et al., *Human-derived organ-on-a-chip for personalized drug development.* Current pharmaceutical design, 2018. **24**(45): p. 5471-5486.
5. Pandey, U.B. and C.D. Nichols, *Human disease models in Drosophila melanogaster and the role of the fly in therapeutic drug discovery.* Pharmacological reviews, 2011. **63**(2): p. 411-436.
6. Gupta, N., et al., *Microfluidics-based 3D cell culture models: Utility in novel drug discovery and delivery research.* Bioengineering & Translational Medicine, 2016. **1**(1): p. 63-81.
7. Mak, I.W., N. Evaniew, and M. Ghert, *Lost in translation: animal models and clinical trials in cancer treatment.* American journal of translational research, 2014. **6**(2): p. 114.
8. Pound, P. and M. Ritskes-Hoitinga, *Is it possible to overcome issues of external validity in preclinical animal research? Why most animal models are bound to fail.* Journal of translational medicine, 2018. **16**(1): p. 1-8.
9. MPharm, D.N., *Microneedle Mediated Optical Detection of Glucose Concentration in Aqueous Solutions*. 2019, Ulster University.
10. Zhao, Y., et al., *Multi-organs-on-chips: towards long-term biomedical investigations.* Molecules, 2019. **24**(4): p. 675.
11. dos Santos, N.A.G., et al., *Cisplatin-induced nephrotoxicity and targets of nephroprotection: an update.* Archives of toxicology, 2012. **86**(8): p. 1233-1250.
12. Kim, L., et al., *A practical guide to microfluidic perfusion culture of adherent mammalian cells.* Lab on a Chip, 2007. **7**(6): p. 681-694.
13. Jang, K.-J., et al., *Human kidney proximal tubule-on-a-chip for drug transport and nephrotoxicity assessment.* Integrative Biology, 2013. **5**(9): p. 1119-1129.
14. Lee, J., K. Kim, and S. Kim, *Kidney on chips.* Methods in cell biology, 2018. **146**: p. 85-104.
15. Chen, Z.-l., et al., *An estimation of mechanical stress on alveolar walls during repetitive alveolar reopening and closure.* Journal of Applied Physiology, 2015. **119**(3): p. 190-201.
16. Mahto, S.K., et al., *Microfluidic shear stress-regulated surfactant secretion in alveolar epithelial type II cells in vitro.* American Journal of Physiology-Lung Cellular and Molecular Physiology, 2014. **306**(7): p. L672-L683.
17. Delon, L.C., et al., *A systematic investigation of the effect of the fluid shear stress on Caco-2 cells towards the optimization of epithelial organ-on-chip models.* Biomaterials, 2019. **225**: p. 119521.
18. Cruzat, V., et al., *Glutamine: metabolism and immune function, supplementation and clinical translation.* Nutrients, 2018. **10**(11): p. 1564.
19. Memic, A., et al., *Bioprinting technologies for disease modeling.* Biotechnology letters, 2017. **39**(9): p. 1279-1290.
20. Walker, P.A., et al., *The evolution of strategies to minimise the risk of human drug-induced liver injury (DILI) in drug discovery and development.* Archives of toxicology, 2020. **94**(8): p. 2559-2585.
21. Gramenzi, A., et al., *Alcoholic liver disease–pathophysiological aspects and risk factors.* Alimentary pharmacology & therapeutics, 2006. **24**(8): p. 1151-1161.
22. Kang, S.M., et al., *Engineered microsystems for spheroid and organoid studies.* Advanced Healthcare Materials, 2021. **10**(2): p. 2001284.

23. Hassan, S., et al., *Liver-on-a-Chip Models of Fatty Liver Disease.* Hepatology, 2020. **71**(2): p. 733-740.
24. Lee, K.-H., J. Lee, and S.-H. Lee, *3D liver models on a microplatform: well-defined culture, engineering of liver tissue and liver-on-a-chip.* Lab on a Chip, 2015. **15**(19): p. 3822-3837.
25. Ortega-Ribera, M., et al., *Nanoengineered Biomaterials for the treatment of liver diseases*, in *Nanoengineered Biomaterials for Regenerative Medicine*. 2019, Elsevier. p. 417-441.
26. Rodriguez-Garcia, A., et al., *3D in vitro human organ mimicry devices for drug discovery, development, and assessment.* Advances in Polymer Technology, 2020. **2020**.
27. Wilson, S.L., M. Ahearne, and A. Hopkinson, *An overview of current techniques for ocular toxicity testing.* Toxicology, 2015. **327**: p. 32-46.
28. Alépée, N., et al., *t4 workshop report: State-of-the-art of 3D cultures (organs-on-a-chip) in safety testing and pathophysiology.* Altex, 2014. **31**(4): p. 441.
29. Hirschhaeuser, F., et al., *Multicellular tumor spheroids: an underestimated tool is catching up again.* Journal of biotechnology, 2010. **148**(1): p. 3-15.
30. Du, Y., et al., *Mimicking liver sinusoidal structures and functions using a 3D-configured microfluidic chip.* Lab on a Chip, 2017. **17**(5): p. 782-794.
31. Li, X., et al., *A glass-based, continuously zonated and vascularized human liver acinus microphysiological system (vLAMPS) designed for experimental modeling of diseases and ADME/TOX.* Lab on a Chip, 2018. **18**(17): p. 2614-2631.
32. Vernetti, L.A., et al., *A human liver microphysiology platform for investigating physiology, drug safety, and disease models.* Experimental biology and medicine, 2016. **241**(1): p. 101-114.
33. Mi, S., et al., *Construction of a liver sinusoid based on the laminar flow on chip and self-assembly of endothelial cells.* Biofabrication, 2018. **10**(2): p. 025010.
34. Ma, L.-D., et al., *Design and fabrication of a liver-on-a-chip platform for convenient, highly efficient, and safe in situ perfusion culture of 3D hepatic spheroids.* Lab on a Chip, 2018. **18**(17): p. 2547-2562.
35. Gori, M., et al., *Investigating nonalcoholic fatty liver disease in a liver-on-a-chip microfluidic device.* PLoS One, 2016. **11**(7): p. e0159729.
36. Karnik, S., et al., *Real-time measurement of cholesterol secreted by human hepatocytes using a novel microfluidic assay.* Technology, 2018. **6**(03n04): p. 135-141.
37. Maschmeyer, I., et al., *A four-organ-chip for interconnected long-term co-culture of human intestine, liver, skin and kidney equivalents.* Lab on a Chip, 2015. **15**(12): p. 2688-2699.
38. Jang, K.-J., et al., *Reproducing human and cross-species drug toxicities using a Liver-Chip.* Science translational medicine, 2019. **11**(517).
39. Asif, A., et al., *Microphysiological system with continuous analysis of albumin for hepatotoxicity modeling and drug screening.* Journal of Industrial and Engineering Chemistry, 2021. **98**: p. 318-326.
40. Farooqi, H.M.U., et al., *Real-time physiological sensor-based liver-on-chip device for monitoring drug toxicity.* Journal of Micromechanics and Microengineering, 2020. **30**(11): p. 115013.
41. Fanning, A.S., et al., *The tight junction protein ZO-1 establishes a link between the transmembrane protein occludin and the actin cytoskeleton.* Journal of Biological Chemistry, 1998. **273**(45): p. 29745-29753.
42. Gonzalez-Mariscal, L., et al., *Tight junction proteins.* Progress in biophysics and molecular biology, 2003. **81**(1): p. 1-44.
43. Srinivasan, B., et al., *TEER measurement techniques for in vitro barrier model systems.* Journal of laboratory automation, 2015. **20**(2): p. 107-126.
44. Jones, C.G. and C. Chen, *An arduino-based sensor to measure transendothelial electrical resistance.* Sensors and Actuators A: Physical, 2020. **314**: p. 112216.

45. Aman, J., et al., *Using cultured endothelial cells to study endothelial barrier dysfunction: Challenges and opportunities.* American Journal of Physiology-Lung Cellular and Molecular Physiology, 2016. **311**(2): p. L453-L466.
46. Nikolic, M., T. Sustersic, and N. Filipovic, *In vitro models and on-chip systems: Biomaterial interaction studies with tissues generated using lung epithelial and liver metabolic cell lines.* Frontiers in bioengineering and biotechnology, 2018. **6**: p. 120.
47. Salih, A.R.C., et al., *Impact of serum concentration in cell culture media on tight junction proteins within a multiorgan microphysiological system.* Microelectronic Engineering, 2020. **232**: p. 111405.
48. Farooqi, H.M.U., et al., *Real-time monitoring of liver fibrosis through embedded sensors in a microphysiological system.* Nano Convergence, 2021. **8**(1): p. 1-12.
49. Chethikkattuveli Salih, A.R., et al., *Extracellular Matrix Optimization for Enhanced Physiological Relevance in Hepatic Tissue-Chips.* Polymers, 2021. **13**(17): p. 3016.
50. Michl, J., K.C. Park, and P. Swietach, *Evidence-based guidelines for controlling pH in mammalian live-cell culture systems.* Communications biology, 2019. **2**(1): p. 1-12.
51. Jang, J., et al., *Colorimetric pH measurement of animal cell culture media.* Biotechnology letters, 2010. **32**(11): p. 1599-1607.
52. Lee, S., et al., *Measurement of pH and dissolved oxygen within cell culture media using a hydrogel microarray sensor.* Sensors and Actuators B: Chemical, 2008. **128**(2): p. 388-398.
53. Kim, D., et al., *Microfluidics-based in vivo mimetic systems for the study of cellular biology.* Accounts of chemical research, 2014. **47**(4): p. 1165-1173.
54. Liu, Y., E. Gill, and Y.Y. Shery Huang, *Microfluidic on-chip biomimicry for 3D cell culture: a fit-for-purpose investigation from the end user standpoint.* Future science OA, 2017. **3**(2): p. FSO173.
55. Xia, L., et al., *Identification of genes required for protection from doxorubicin by a genome-wide screen in Saccharomyces cerevisiae.* Cancer research, 2007. **67**(23): p. 11411-11418.
56. Gyöngyösi, M., et al., *Liposomal doxorubicin attenuates cardiotoxicity via induction of interferon-related DNA damage resistance.* Cardiovascular research, 2020. **116**(5): p. 970-982.
57. Wainberg, Z.A., et al., *Lapatinib, a dual EGFR and HER2 kinase inhibitor, selectively inhibits HER2-amplified human gastric cancer cells and is synergistic with trastuzumab in vitro and in vivo.* Clinical Cancer Research, 2010. **16**(5): p. 1509-1519.
58. Flannery, P.C., K.L. Abbott, and S.R. Pondugula, *Correlation of PPM1A downregulation with CYP3A4 repression in the tumor liver tissue of hepatocellular carcinoma patients.* European journal of drug metabolism and pharmacokinetics, 2020. **45**(2): p. 297-304.
59. Lau, Q.Y., et al., *In vivo-Like Hierarchical Coculture of Hepatocytes, Hepatic Stellate Cells, and Sinusoidal Endothelial Cells for TGF-b-Induced Early Liver Fibrosis Studies in vitro.* 2020.
60. Fletcher, E.S., *ORGAN SPECIFIC VASCULAR RESPONSE TO FIBROSIS AFFECTS BREAST CANCER METASTATIC ORGANOTROPISM.* 2016.
61. Yang, L., et al., *Hydrophilic cell-derived extracellular matrix as a niche to promote adhesion and differentiation of neural progenitor cells.* RSC advances, 2017. **7**(72): p. 45587-45594.
62. Halper, J. and M. Kjaer, *Basic components of connective tissues and extracellular matrix: elastin, fibrillin, fibulins, fibrinogen, fibronectin, laminin, tenascins and thrombospondins.* Progress in heritable soft connective tissue diseases, 2014: p. 31-47.
63. Choy, H.A., et al., *Physiological osmotic induction of Leptospira interrogans adhesion: LigA and LigB bind extracellular matrix proteins and fibrinogen.* Infection and immunity, 2007. **75**(5): p. 2441-2450.